Magnetic and Thermal Imaging with Novel Quantum Microscopy

Cheng, Zhiyuan

Magnetic and Thermal Imaging with Novel Quantum Microscopy

THESIS

submitted in partial fulfillment of the
requirements for the degree of

MASTER OF SCIENCE
in
PHYSICS

Author :	Zhiyuan Cheng
Student ID :	2673568
Supervisor :	Jan Aarts & Kaveh Lahabi
Second corrector :	Wolfgang Löffler

Leiden, The Netherlands, September 4, 2022

Magnetic and Thermal Imaging with Novel Quantum Microscopy

Zhiyuan Cheng

Huygens-Kamerlingh Onnes Laboratory, Leiden University
P.O. Box 9500, 2300 RA Leiden, The Netherlands

September 4, 2022

Abstract

The scanning quantum interference device (SQUID) on tip (SoT) has shown promising features of high spatial resolution and magnetic field sensitivity. Present day implementations of the SoT lacks proper height control and topography feedback. Several techniques for realizing a SoT have been shown, however a challenge that remains is to design a reliable and efficient method for fabricating electrical contacts that reach the SQUID. Directly sputtered multi-layers for SQUID fabrication can always create a short circuit between the excitation circuit and the read-out circuit due to high temperature during sputtering and the porous and unstable structure of silver epoxy contacts on the Akiyama-probes. Therefore, we explored the option of depositing the layers onto the probes via float transfer, which avoids high temperature. As a result, the transferred layers are well attached to most area of the probe except the tip. Nevertheless, float transfer can be a promising method to deposit metal layers for electrical contacts without creating short circuits. Further studies of acquiring floating layers with flatter surface combining with other layer deposition techniques are suggested.

Contents

1 Introduction **1**

2 Theory **3**
2.1 SQUID 3
2.2 Scanning SQUID Microscopy 5
2.2.1 Resolution 6
2.3 SQUID-on-Tip 7
2.4 Akiyama-Probe 11

3 Method 1: Sputtering deposition **15**
3.1 Sputtering with hard mask 15
3.2 Adding more insulating layers 17
3.2.1 Adding a PMMA layer 17
3.2.2 Adding Torr seal 19
3.2.3 Annealing 22

4 Method 2: Float transfer **25**
4.1 Introduction to float transfer 25
4.2 Sputtering onto a copper foil 26
4.3 Encapsulating the multi-layers 29
4.4 Floating layers on probe 31

5 Conclusions and Outlooks **37**

6 Acknowledgement **39**

Version of September 4, 2022– Created September 4, 2022 - 22:42

Chapter 1

Introduction

The frontier research in condensed matter physics has gone to atomic or even sub-atomic scales, which put a challenge to the current probing methods for a more precise knowledge of the electric and magnetic fields. Superconductors are extremely sensitive to the presence of electric and magnetic field, this property makes them the ideal candidate of materials for field sensors. One of the electric and magnetic sensors based on this property is the Superconducting Quantum Interference Device (SQUID), a superconducting loop with two Josephson Junctions (JJ).

Ever since 1970s, SQUID magnetometers have been applied to detect weak magnetic fields in various experiments[1]. The Scanning SQUID Microscope (SSM) was therefore developed for magnetic field probing and imaging[1]. However, the SSM has a limited spatial resolution and magnetic sensitivity due to its use of large pick-up loop coils, which has a typical diameter of several micrometers[1, 2], and large coil-to-sample spacing, which is usually several micrometers[1]. More recent in 2010, *E. Zeldov et al.* fabricated a self-aligned nanoscale SQUID on the tip of a pulled quartz capillary, known as the SQUID on Tip (SoT)[3]. The SoT has an effective diameter varying from 39 nm[4] to several hundred nanometers[3], which is several orders of magnitude smaller than SSM. The working distance between the tip and the sample is usually below 1 μm[3]. Therefore, the spatial resolution and magnetic sensitivity were significantly improved due to a much smaller loop size and tip-to-sample distance. Additionally, SoT can also be used as a thermometer to probe and image temperature of the sample, whose sensitivity is 4 to 5 orders of magnitude better than other commonly used thermometers[5]. By combining SoT with Scanning Probe Microscopy (SPM), *Poggio et al.* developed a SoT on an AFM cantilever, which enables high-resolution topography while probing magnetic fields

Version of September 4, 2022– Created September 4, 2022 - 22:42

and temperature of the sample at the same time[6]. Therefore, fabricating high-resolution SoT on a scanning probe enables physics research at a much smaller scale, where new fundamental physics concepts can be found. And thus, this encourages my research on how to make electrical contacts to the SQUIDs on the tips of the cantilevers.

Chapter 2

Theory

In this chapter, we will present some background theory for the SQUID, SSM and SoT so that the basic work principles can be well understood. This also presents additional motivation for my project.

2.1 SQUID

In a conventional superconductor, electrons form a condensate of Cooper pairs. This condensate can be described by a singular wavefunction:

$$\Psi = |\Psi_0| \cdot e^{i\delta} \tag{2.1}$$

where δ is the phase factor of the wavefunction. Unlike classical electronics, in which currents are driven by the bias, the current in a superconductor is determined by the phase difference, namely:

$$I = I_0 \cdot \sin \Delta\delta \tag{2.2}$$

where I_0 is the critical current of the superconductor, and $\Delta\delta$ is the phase difference in the superconductor.

A JJ consists of two superconductors coupled by a weak link (WL). By cooling down the JJ below the transition temperature, the wavefunctions in the two superconductors start to overlap in the WL, and supercurrent driven by the phase difference between two superconductors can be generated. Generally, there are various types of WL's, such as constriction and S-N-S, *etc.*. In our set-up, the S-N-S is used to avoid hysteresis in the I-V sweep as spin relax time is much smaller.

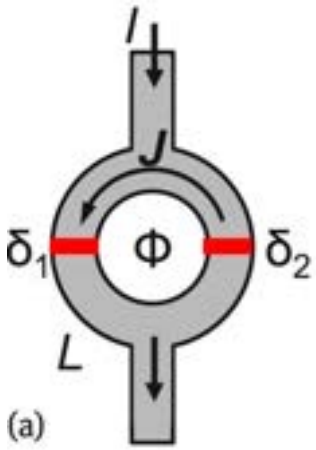

Figure 2.1: *Schematic of a SQUID. WL's are marked in red. The magnetic flux, Φ in the SQUID loop can lead to a quantum phase difference ($\Delta\delta = \delta_2 - \delta_2$) of the two JJ's. Figure is taken from D. Köller et al., 2017 [7].*

The working unit of a SQUID has two independent JJ's in a parallel circuit (shown in figure 2.1). From equation 2.2, the current in a SQUID can be characterized by the phase difference between two JJ's:

$$I = I_0 \cdot \sin\left(\delta_2 - \delta_1 + 2\pi\frac{\Phi}{\Phi_0}\right) \tag{2.3}$$

where δ_1 and δ_2 are the phases of the two JJ's, Φ is the magnetic flux introduced to the SQUID and Φ_0 is the magnetic flux quantum[7].

As a result, there is a supercurrent, J, circulating in the SQUID loop. Since the SQUID has a certain critical current I_0, above which superconductivity is compromised and the superconductor transitions into a normal conductor, introducing an extra bias current I_b to the SQUID loop will lead to an oscillation with the magnetic flux. Figure 2.2(a) shows the critical current lowered by the presence of the magnetic flux and figure 2.2(b) shows the bias current oscillating with the magnetic flux.

The I-V characteristics are non-linear in the presence of magnetic flux, this implies that a slight change of the flux introduced into the SQUID loop will change the I-V read-out dramatically. Such mechanism makes the SQUIDs to be highly sensitive to magnetic field. Moreover, the I-V characteristics are well studied and characterized, which enables the quantitative description of the change in field. One example of application the SQUID sensor is the Scanning SQUID Microscopy (SSM), which enables magnetic probing and imaging.

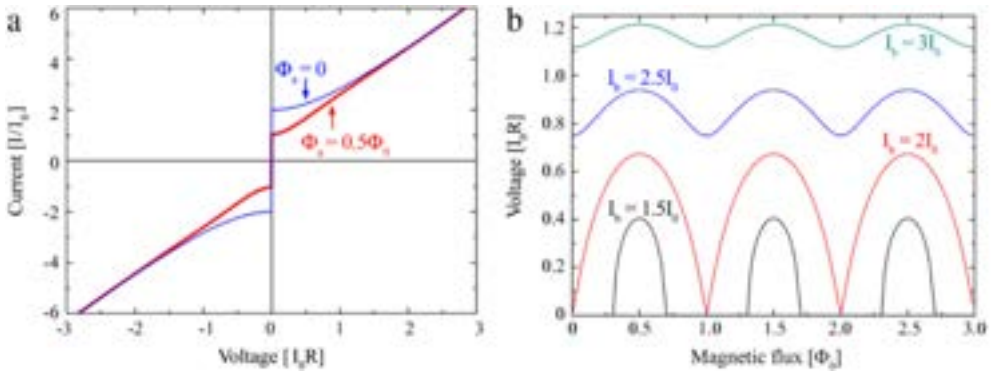

Figure 2.2: *I-V measurements of a SQUID and how the magnetic flux influences the I-V relations. (a) The blue and red curves show the I-V features of a SQUID with respect to no flux and half flux quantum ($0.5\Phi_0$) presence. With a presence of magnetic flux, the critical current of the SQUID can be lower than that without flux. (b) The voltage, characterized by current multiplied by resistance, is oscillating periodically with the magnetic flux. I_0 is the critical current and I_b is the bias current, which corresponds to I in figure 2.1. Figure is taken from A. Vettoliere et al., 2016 [8].*

2.2 Scanning SQUID Microscopy

Figure 2.3 shows the schematic structure of SSM loop. The loop has two main units - a SQUID consisting two JJ's and a pickup loop (figure 2.3(a)). By inserting the pickup loop at a distance h above the sample with a tilted angle θ, the SSM can pick up magnetic field from the sample (figure 2.3(b)). The probe can scan along the surface with a scanning step defined by Δx and Δy, which are determined by the piezo actuators. Since the scanning steps are normally smaller than the diameter of the pickup coil (figure 2.3(c)), the spatial resolution of the SSM is limited by the size of the pickup loop[9]. Due to Meissner effect, there will be more field collected by the coil, leading to a slightly larger effective area than the inner area of the coil (figure 2.3(d))[9]. Hence, the local magnetic field can be characterized by equation modified from equation 2.3:

$$I = I_0 \cdot \sin\left(\Delta\delta + 2\pi \frac{\boldsymbol{B} \cdot \boldsymbol{A_e}}{\Phi_0}\right) \tag{2.4}$$

where $\boldsymbol{B}$ is the magnetic field and $\boldsymbol{A_e} = |A_e| \cdot \boldsymbol{n_A}$ is the effective area of the probe loop. Despite all the fundamental limitations mentioned above, *H. Hilgenkamp et al.* managed to image vortices in a YBCO film (figure 2.4(a))[10].

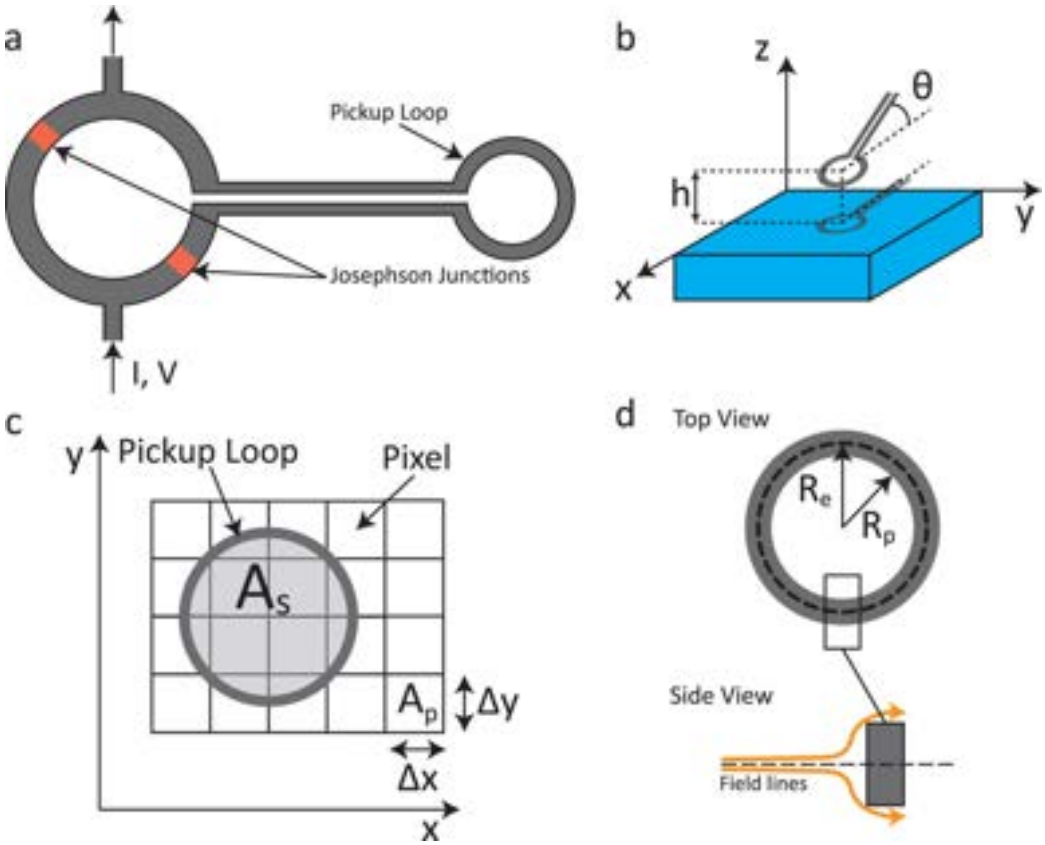

Figure 2.3: *(a) A schematic of SSM. (b) SSM probes a sample with a pickup loop at an angle of θ and a height of h. (c) Comparison of the pickup loop size and pixel size. (d) Schematic of magnetic field distribution near the superconductor. This leads to a larger effective area than the inner area of the loop. Figure is taken from H. Hilgenkamp et al., 2017 [9].*

2.2.1 Resolution

The typical spatial resolution of SSM is normally several micrometers[11–13]. The state-of-the-art SSM probe from *Kirtley et al.* reaches sub-micron resolution by implementing fine design with more shielding layers[13, 14]. The spatial resolution of the probe is mainly limited by both the diameter of the probe, d, and the loop-to-sample distance, h (figure 2.4(b))[9]. From *J. R. Kirtley et al., 1999* [1], equal probe diameter and scanning height ($h = d$) provide the best combination of spatial resolution and field sensitivity, which is also shown in figure 2.4(b).

The effective diameter of the SSM is at micrometer scale, most of which is contributed by the pick-up loop. According to equation 2.4, larger loop

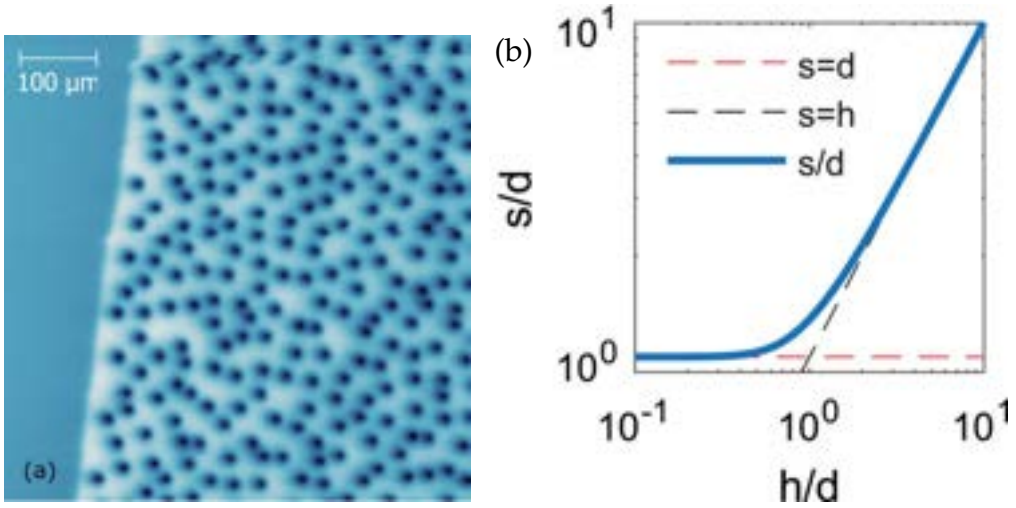

Figure 2.4: *(a) Vortices (black) in a 200 nm thick YBCO film imaged by a SSM probe at a field of 6.93 μT and temperature of 4 K. Figure is taken from H. Hilgenkamp et al., 2015 [10]. (b) The normalized spatial resolution (s/d) as a function of h/d (blue solid line) with the limits of $s = d$ (red dashed line) and $h = d$ (black dashed line). s represents the spatial separation of two out-of-plane field extrema. Figure is taken from H. Hilgenkamp et al., 2017 [9].*

area can lead to worse field sensitivity. Simultaneously, d is normally at micrometer scale, which becomes a limitation for better resolution and sensitivity even at much smaller scanning height. Therefore, reducing the size of the probe to sub-micron scale can improve the spatial resolution and sensitivity greatly.

2.3 SQUID-on-Tip

To further reduce the total area of the SQUID loop, *E. Zeldov et al.* developed a new scanning SQUID microscopy technique by implementing pulled glass capillaries sputtered with Pb to form constriction WL's, which is known as the SQUID-on-Tip (SoT)[3]. Without a large pickup loop, the SQUID loop itself is the picking up the magnetic field, which has a diameter of 600 nm[3]. With much smaller effective area of 0.034 μm^2, this SoT can exhibit a flux sensitivity of $1.8 \times 10^{-6}\Phi_0/\text{Hz}$[3], which is slightly smaller than the sub-micron SSM from *Kirtley et al.*[14]. Given the fact that this SoT has a scanning height of more than 1 μm[3] which is much larger than the scanning height of 0.33 μm in the sub-micron SSM[14], the improvement of field sensitivity is promising.

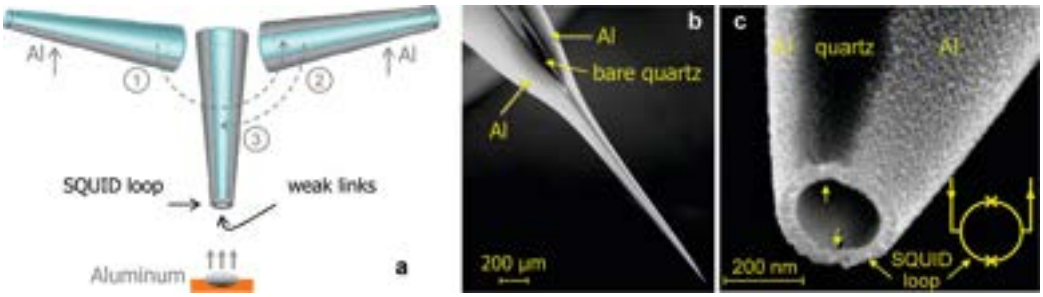

Figure 2.5: *(a) Schematic of fabrication of SoT by 3 steps of evaporating aluminium onto the pulled quartz capillary tip. (b) and (c) are the SEM images of the tip. The two regions (marked by the yellow arrows in (c)) on the ring form the two WL's of the SQUID. Schematic SQUID loop is shown as the inset of (c). Figure is taken from E. Zeldov et al., 2010 [3].*

By applying a tuning fork for height feedback and smaller effective area, *Zeldov et al.* also realized SoT's with single spin sensitivity[4, 15].

SoT is also capable of thermal imaging. Since the current can change dramatically near T_c, this enables thermal SoT (tSoT) to image temperature distribution of the sample. The superconductor is an ideal thermal insulator, the whole measuring system of SoT is mostly thermal insulated from the environment except the tip for readout, which makes probing with tSoT non-invasive. By introducing an exchange Helium gas, the tSoT is thermally weak-linked to the sample, and thermal information could be read out from the I-V measurements (figure 2.6(c))[5]. From figure 2.6(a), the tSoT is four orders of magnitude more sensitive than any other thermal probing techniques[5], which makes it an exceptional thermal probing microscope.

Moreover, *Zeldov et al.* also developed a 3-junction SoT, which is capable to measure in-plane magnetic field[16].

So far, the SoT has proved itself to be a promising probing technique for both magnetic and thermal imaging. Yet, due to the stiffness of quartz capillary, this SoT lacks ideal feedback of height and sample topography. And one solution to this is to combine the SoT with SPM.

An example of SoT on a scanning probe is the recent work from *Poggio et al.*[6]. First, a clean AFM cantilever (Figure 2.7(a)(i)) is patterned by focus ion beam (FIB) milling, leaving a triangular plateau at the tip of the cantilever (figure 2.7(a)(ii)). Then a thin film of *Nb* is deposited onto the cantilever (figure 2.7(a)(iii)), which is later FIB milled into a SQUID loop (figure 2.7(a)(iv)) protected with a shunt *Pt* resistor (figure 2.7(d))[6].

Figure 2.8 shows the topography, magnetic and thermal map of a current-

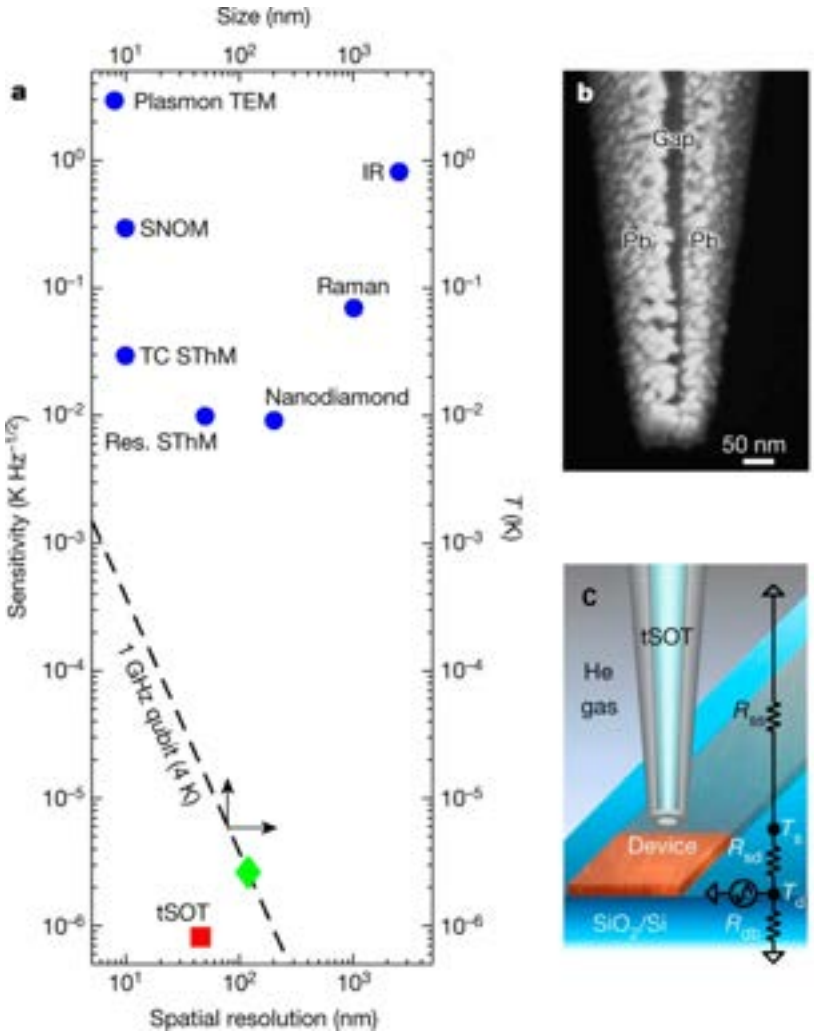

Figure 2.6: *(a) Sensitivity (left-hand vertical axis) of various thermal imaging techniques (blue) and tSoT (red) with respect to the spatial resolution (horizontal axis). The black dashed line and green diamond correspond to the theoretical scaling of temperature increase (right-hand vertical axis) of a qubit operation at Landauer's limit. (b) SEM image of the Pb tSoT with an effective diameter of* 46 nm. *(c) Schematic image of tSoT thermal probing. Helium gas is introduced for weak thermal link between the sample and tSoT. The inset shows the effective thermal circuit. Figure is taken from E. Zeldov et al., 2016 [5].*

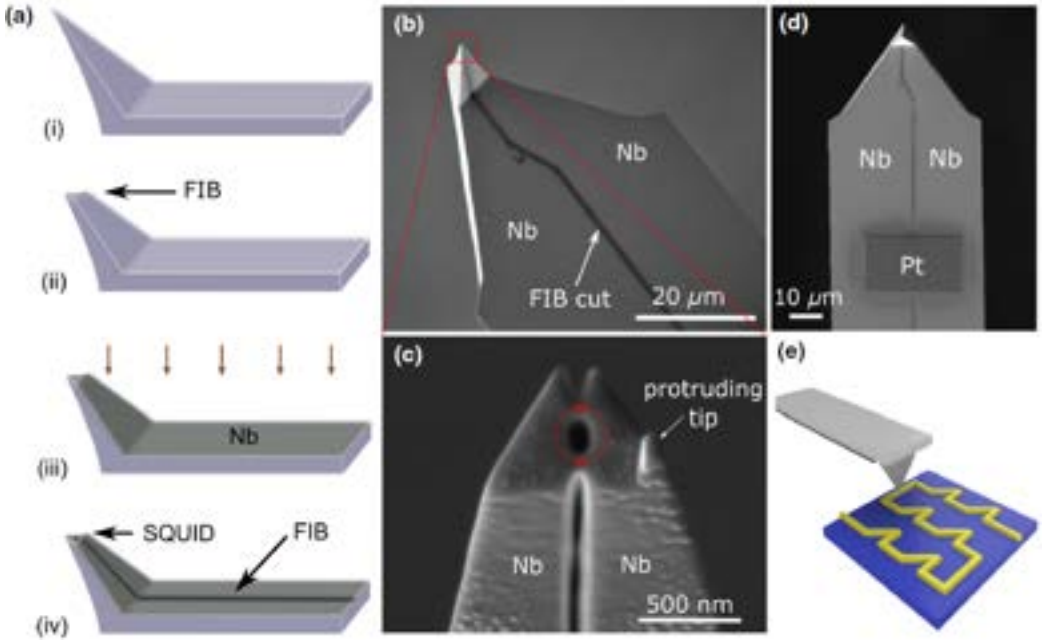

Figure 2.7: *(a) Schematics of fabrication process of SoT on AFM cantilever. First, (ii) the tip of the cantilever is milled away by focused ion beam (FIB), leaving a triangular plateau. Then (iii) a thin layer of Nb is deposited onto the cantilever and (iv) a hole and trench is directly milled through the Nb layer, forming a SQUID on the tip shown in (c). (b), (c) and (d) show the SEM image of the SoT on AFM cantilever, the protruding tip in (c) is also patterned by FIB milling, and the Pt film is a shunt resistor protecting the SQUID loop. (e) Schematics of the scanning probe and sample. Figure is taken from M. Poggio et al., 2022 [6].*

carrying 120-nm thick gold wire. From figure 2.8(c), the current density map can be retrieved by Biot-Savart law[6]. Moreover, a recent application of this SoT on AFM cantilever successfully imaged the current distribution in a qubit loop, providing insight to qubit control optimization[17].

2.4 Akiyama-Probe

In previous sections, we have learnt that the SoT can be a promising probing technique. However fabricating SoT on a cantilever, especially making electrical contacts to the SQUID on the cantilever tip takes a lot of effort. Also, due to lack of proper tip structure, the SoT on AFM cantilever by *Poggio et al.* exhibits double visions in AFM topography[6]. Therefore, making SoT's with proper tip structure is vital for further observation at much smaller scales with higher resolution and sensitivity.

In our set-up, we use a commercially available *Akiyama AFM Probe* from NANOSENSORS™. The Akiyama-Probe has a tuning fork with two separate arms (figure 2.9), which can be used for making an extra circuit on the probe. As the two arms are separated, we do not need to FIB mill long trenches to separate the contacts, which is advantageous with regard to time-efficiency and effort. And with the previous works by Timothy and Tunde, we can already use electron beam induced deposition (EBID) to print SQUIDs. A recent work by Matthijs also enables us to pattern S-N-S SQUIDs on multi-layers deposited onto the cantilever by using FIB milling. Hence the current urgent mission is to make reliable electrical contacts, which becomes the motivation of my project.

Version of September 4, 2022– Created September 4, 2022 - 22:42

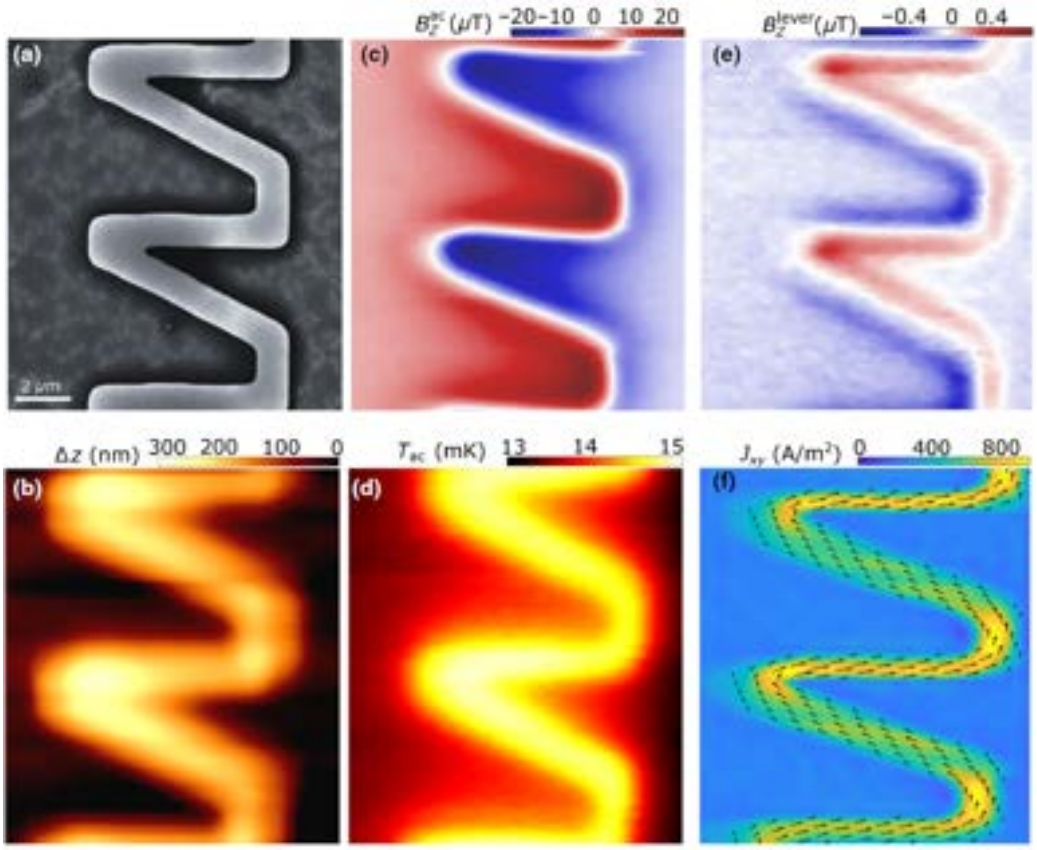

Figure 2.8: *Images of a current-carrying wire. (a) SEM image of a Au wire with a thickness of* 120 nm *patterned on a silicon substrate. (b) Non-contact SoT AFM image showing a topography (*$\Delta z = 140\,\text{nm}$*) of sample at a scanning height of* 140 nm*. (c) Out-of-plane magnetic field* B_z^{ac} *and (d) temperature* T_{ac} *are acquired by probing at a fixed height of* $h = 345\,\text{nm}$*. (e) Out-of-plane magnetic field* B_z^{lever} *probed by actuating the cantilever's fundamental frequency* $f_0 = 282\,\text{kHz}$ *with an amplitude of* 15 nm*. (f) Map of current density* $\boldsymbol{J_{xy}}$ *calculated from* B_z^{ac} *in (c). Figure is taken from M. Poggio et al., 2022 [6].*

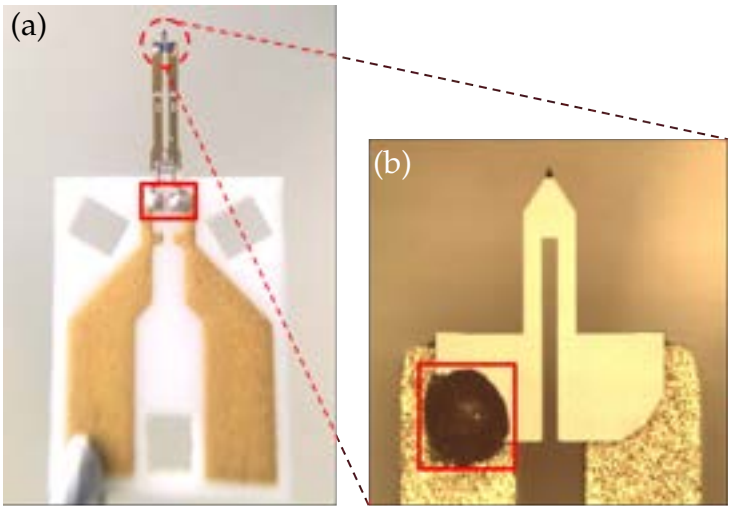

Figure 2.9: *(a) Overview of the Akiyama-Probe. There are two gold contacts on the ceramic plate connected to the two arms of the tuning fork by the two silver epoxies (marked by red box). The two gold contacts are insulated from each other. (b) Overview of the cantilever. There is also another silver epoxy contact (red box) on the cantilever. The cantilever is made of silicon and mounted at the end of the tuning fork with a silver epoxy. The images are taken from the product guide from the supplier[18].*

Chapter 3

Method 1: Sputtering deposition

3.1 Sputtering with hard mask

The initial approach to fabricate a probe with multi-layers was to directly sputter layers onto the probe using a hard mask (figure 3.1(a)). First, we can sputter SiO_x onto the probe without the hard mask. This is mainly to create an insulating layer that separates the SQUID read-out circuit from the tuning fork excitation circuit. In the next step, 4 metal layers are sputtered onto the probe with the use of a hard mask. Generally, to make a S-N-S SQUID, only two layers are needed - the superconducting layer and the normal metal layer for the weak links (WL). However, due to poor adhesion between Pt and SiO_x, we need to add a thin layer of $MoGe$ as a sticking layer to make sure the other layers adhere to the SiO_x surface. A thin layer of Pt is deposited on top on top to reduce the oxidation process of $MoGe$ when exposed to air.

In our sputtering set-up, the sputtering deposition is isotropic (shown in figure 3.1), hence we applied a hard mask mainly to shield the backside of the probe as well as to separate the two arms of the tuning fork to create a circuit. The tip of the cantilever is delicate, and some spaces between the cantilever and hard mask shall be left for the tip in precaution of breaking it. Hence, there will also be conductive materials sputtered at the backside of the tip. In order to remove the layers on backside of the cantilever, we used Ar ion beam etching (IBE) to remove the metal layers on the backside.

In this process, the two gold contacts remain insulated after SiO_x sputtering. However, the contacts become short-circuited after sputtering 4 metal layers. We assume this might be due to insufficient thickness of SiO_x, so thicker layers of SiO_x varying from 50 nm to 200 nm was sputtered, however the gold contacts remained short-circuited. Hence, there

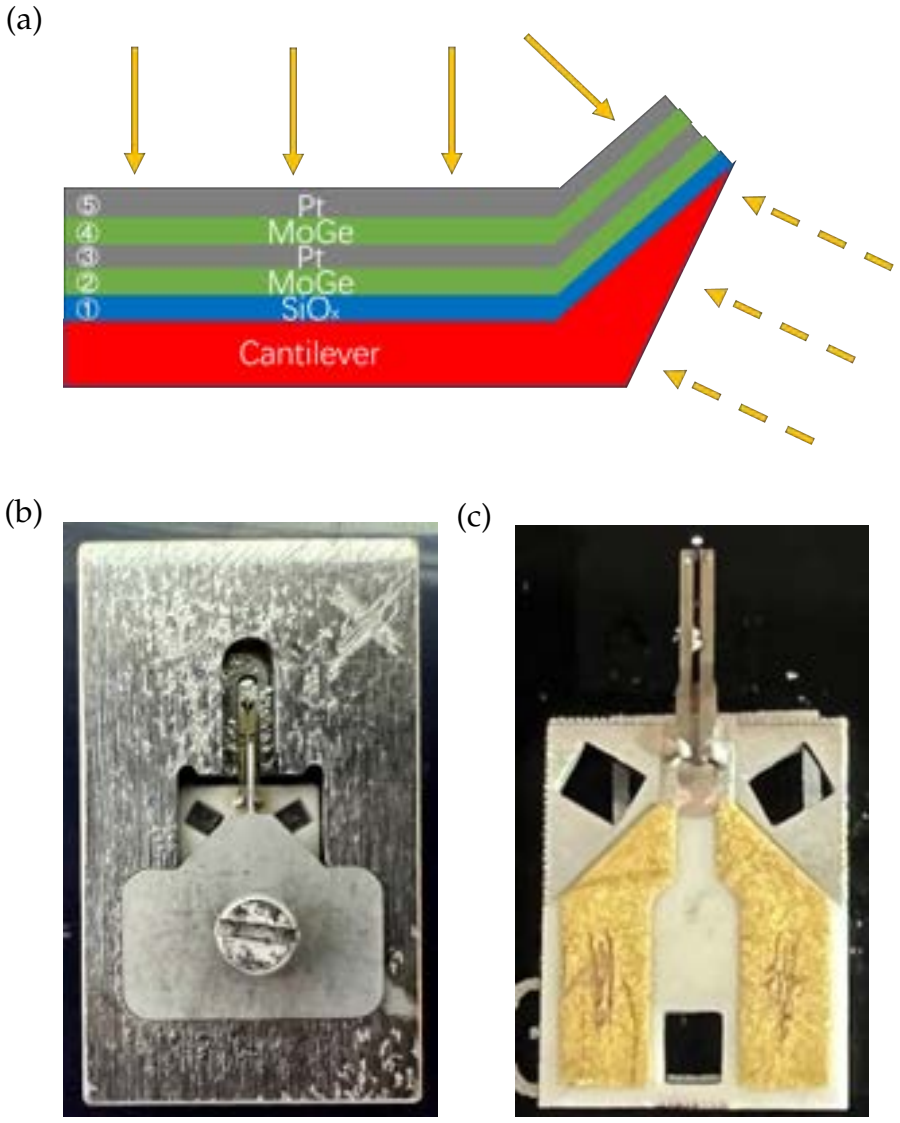

Figure 3.1: *(a) Schematic of sputtering deposition. There are 5 layers sputtered onto the cantilever -* ***1.*** *SiO_x as an insulating layer to separate the SQUID read-out circuit from the tuning fork excitation circuit,* ***2.*** *MoGe as an adhesive layer for better adhesion between the SQUID loop and the cantilever,* ***3.*** *Pt as the normal metal (WL),* ***4.*** *MoGe as the superconducting layer and* ***5.*** *Pt as a capping layer for protection. Yellow arrows represent the sputtering directions. Yellow dashed arrows show that sputtering is isotropic and the backside of the cantilever can also be sputtered. (b) Photo of the hard mask with a cantilever. (c) Probe after sputtering with the hard mask.*

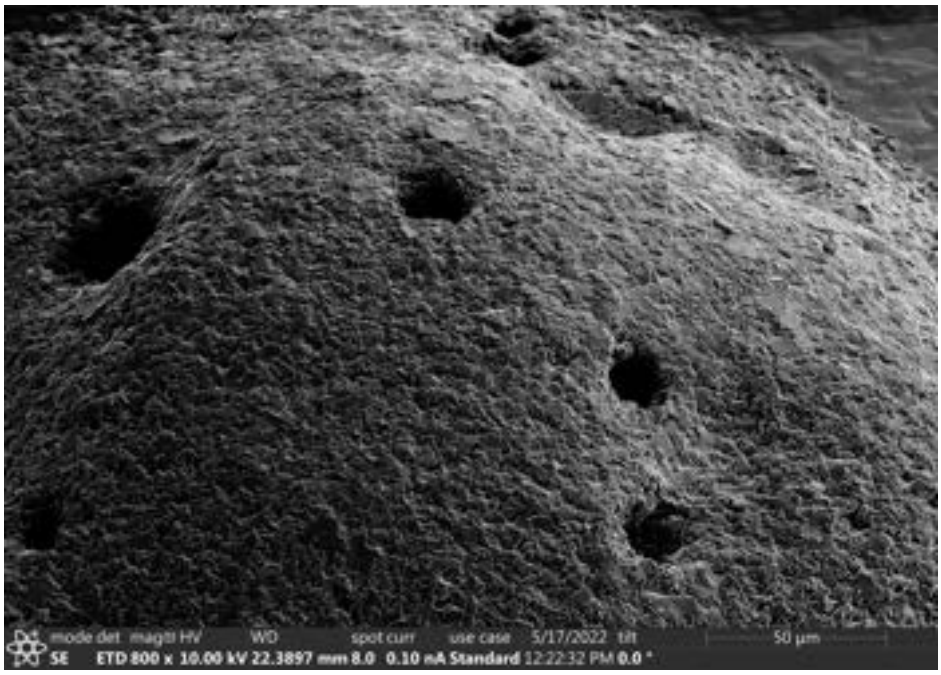

Figure 3.2: *SEM image of a silver epoxy contact, which has a rough surface and porous structure.*

might be something on the probe that creates shorts.

In figure 2.9, there are three silver epoxy contacts on the probe - two mounting the tuning fork onto the ceramic plate which make electrical contact to the tuning fork, one mounting the cantilever at the end of the tuning fork. In the scanning electron microscope (SEM), we noticed that these silver epoxy contacts have a rough surface with porous structure (figure 3.2). Such porosity could limit the deposition of SiO_x, lack of which will create direct contact between gold contact and the multi-layers. Hence we need to cover the silver epoxy contacts for insulation.

3.2 Adding more insulating layers

3.2.1 Adding a PMMA layer

Changing the structure of the hard mask could be problematic, since there is one silver epoxy contact on the cantilever, and using a hard mask to cover it could break the cantilever. Our first approach is to drop poly-methyl methacrylate (PMMA) onto the silver epoxy contacts in hope to form an insulating layer as well as smooth their rough surfaces. Using

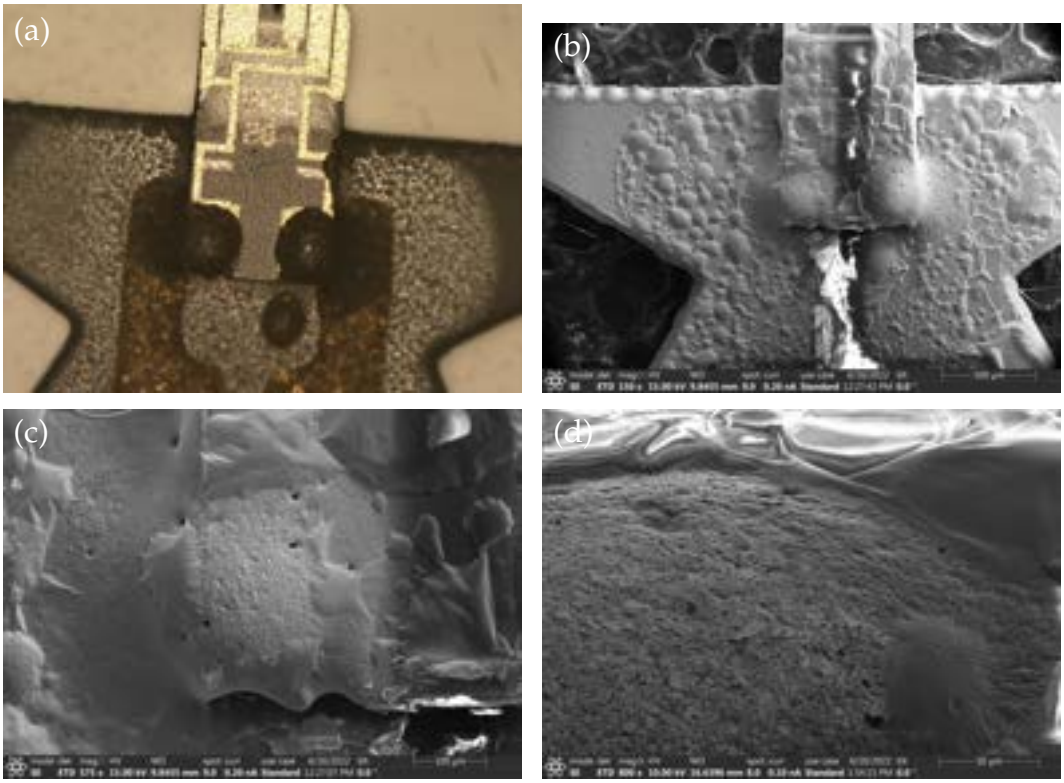

Figure 3.3: *(a) Optical image of PMMA covering the silver epoxy contacts on the tuning fork (before sputtering SiO_x). The bright bubbly area surrounding the silver epoxy contacts shows the deposition of PMMA layer. (b) and (c) shows the overview of PMMA covering the silver epoxy contacts in SEM (after sputtering SiO_x), the PMMA layer forms bubbles. (d) is the zoomed-in tilted image of the silver epoxy contact (after sputtering SiO_x). PMMA layer seems not to cover the silver epoxy contact and the epoxy surface is still rough.*

PMMA can be much safer compared to using a hard mask, because this is less aggressive and the cantilever can be well protected. After 5 minutes of curing at 180 °C, a layer of PMMA seemed to be formed (figure 3.3(a)). Then the probe was sent to be sputtered with 100 nm SiO_x.

However, after SiO_x was sputtered, SEM images (figure 3.3(b) to (d)) show that the silver epoxy contacts were not covered with PMMA, and holes in the epoxy can be seen clearly. The cantilever was then put in the hard mask and ready to be sputtered with metal layers. After the steps above, resistance between contacts was measured and all the contacts were still shorted, which confirmed our initial expectations. Changing the order, i.e. starting with SiO_x sputter deposition and subsequently covering the contacts with PMMA, was similarly ineffective in providing an insu-

lating layer. There are mainly two reasons for the shorted circuits between the contacts. First, PMMA is not dry-etching tolerant enough. During sputtering, *Ar* ions are used to bombard the sputtering target so that a gas of target atoms is formed, which can then be deposited onto the probe. However, during this process, the PMMA layer is also bombarded and destroyed. Secondly, air might be trapped in the silver epoxy contacts due to the porosity of epoxies, which makes it hard for PMMA to fill the holes. Also, the sputtering chamber is pumped down to high vacuum during sputtering, then the air trapped in the silver epoxy contact may destroy the PMMA sealing to escape.

As PMMA is not strong enough to stay on the silver epoxy contacts, we need a much more dry-etching tolerant material to seal the holes in the silver epoxy contacts.

3.2.2 Adding Torr seal

The Torr seal is also an epoxy which is a very stiff material after curing. Unlike the silver epoxy, it does not form holes on its surface. Moreover, the Torr seal can still be well attached to the surface and remain insulating at low temperature. These properties make the Torr seal an ideal candidate material for making an insulating layer to cover the silver epoxy contacts.

Figure 3.4(a) shows the the cured Torr seal layer on top of the silver epoxy contact. Since the cured Torr seal is very stiff, it is not possible to use the old hard mask to make separated contacts. One solution to this is to use a hand-made mask made of Kapton tape, which can remain stable under high temperature during sputtering (shown in figure 3.4(b) and (c)). During gluing the Kapton tape stripe onto the tuning fork, the stripe was carefully placed to cover the silver epoxy contact on the cantilever because applying Torr seal may be too risky to break the cantilever. Figure 3.4(d) shows the probe after all layers were sputtered. From its appearance, the contacts are well separated, which can also be clearly seen in figure 3.5(a) and (b).

However, the SQUID read-out circuit and tuning fork excitation circuit were still shorted. As we turned the probe over, we noticed there are two more silver epoxy contacts that were never considered before (figure 3.5(c)). This could indicate that the short can also come from these two silver epoxy contacts. To further prove this, we ran a test by breaking the top end of the tuning fork along with the cantilever, and thus only leaving two silver epoxy contacts on the front side of the tuning fork (shown in figure 3.6). Then we redo the same process again with Torr seal and Kap-

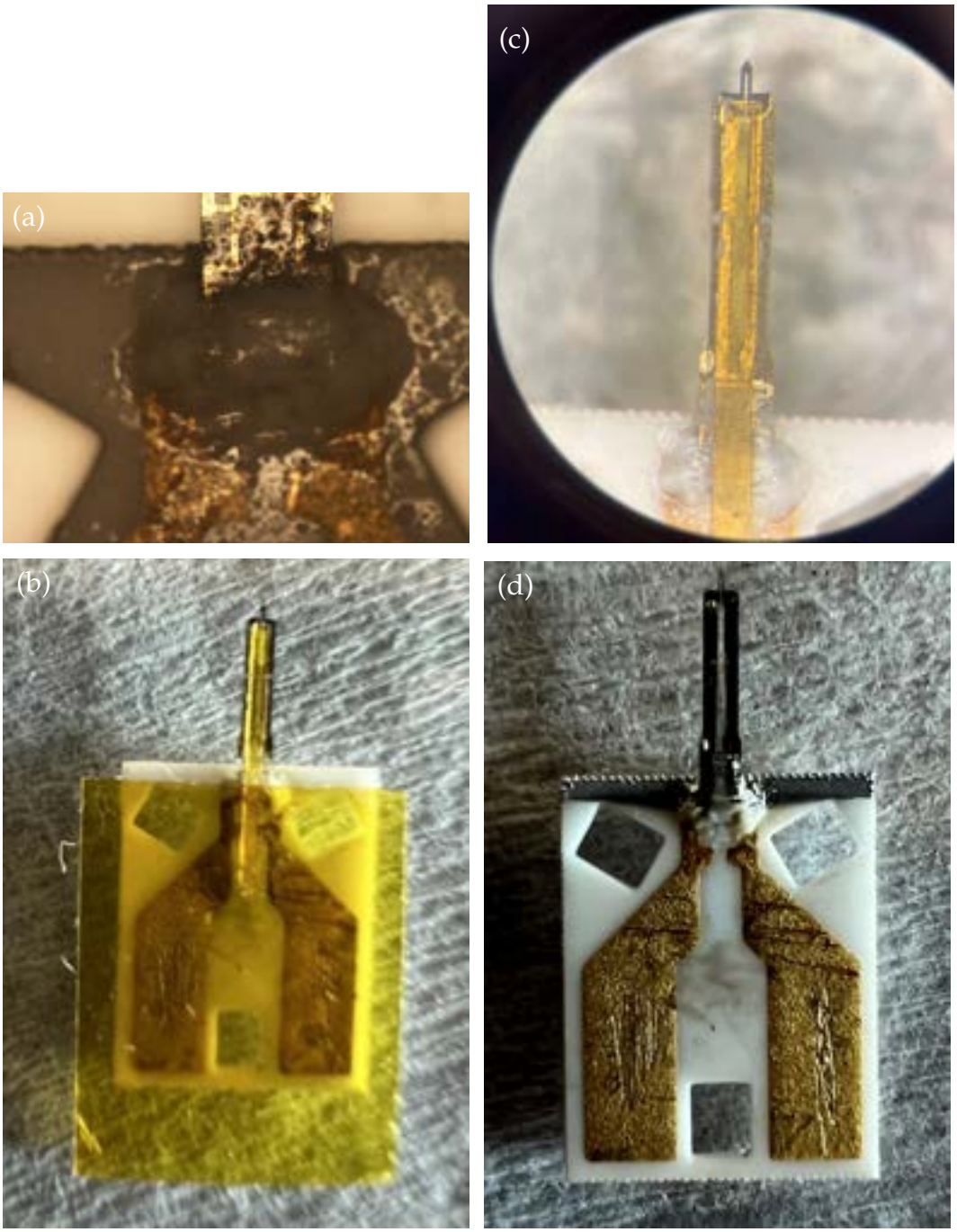

Figure 3.4: *(a) Optical image of cured Torr seal (grey) covering silver epoxy contacts on the tuning fork. (b) Custom-made Kapton mask. (c) Stripe of Kapton tape on the tuning fork to separate the two arms of the tuning fork. (d) Overview of the probe after sputtering multi-layers (after the Kapton mask was removed).*

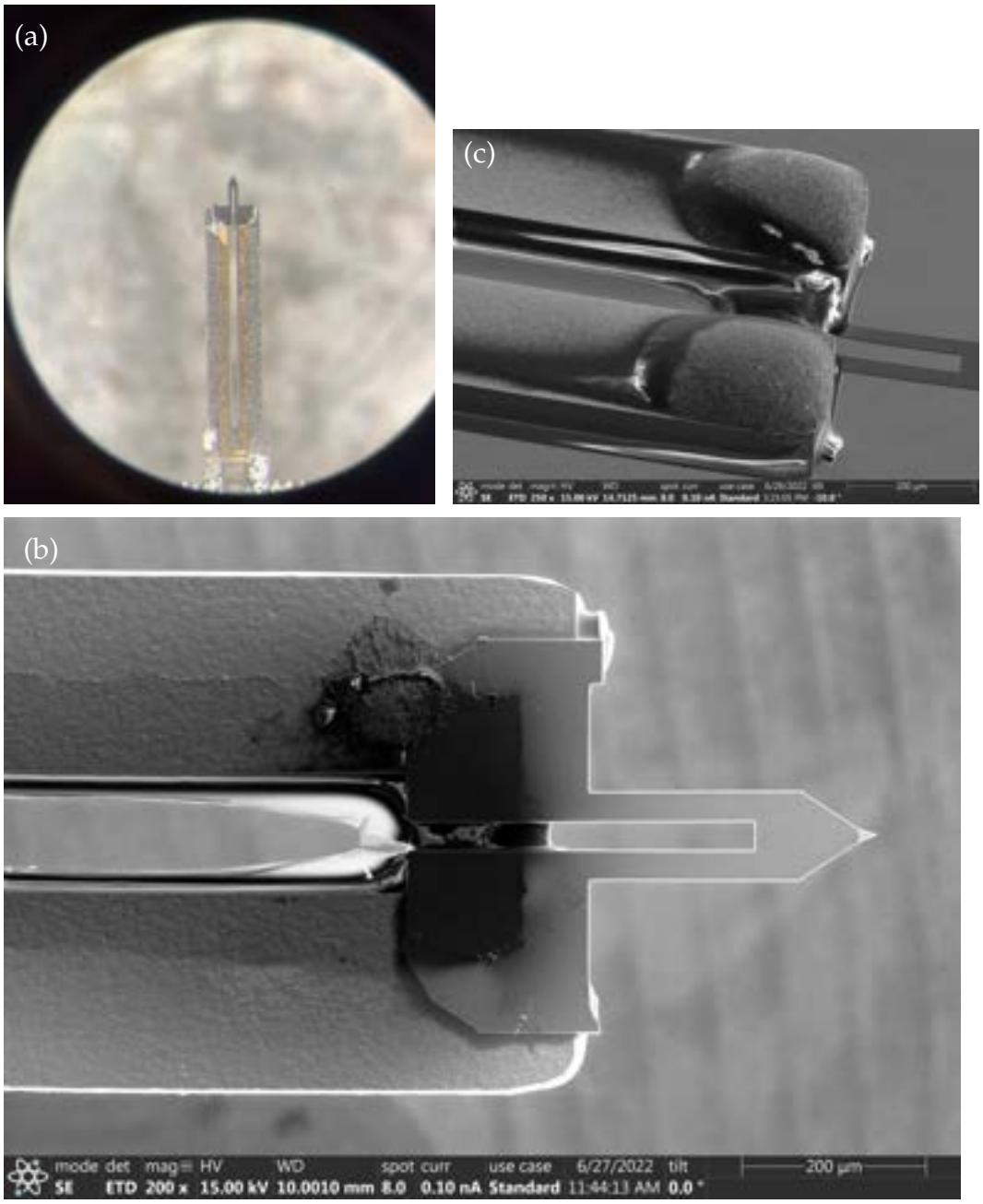

Figure 3.5: *(a) Optical image of the tuning fork after sputtering. Area once covered with Kapton stripe shows the color of gold while that uncovered shows grey metallic color, indicating two arms are separated. (b) SEM image of the cantilever and tuning fork. There is a clear contrast between areas once covered and uncovered with Kapton tape. This also indicates most part of the silver epoxy contact on the cantilever was also covered with Kapton tape and thus not sputtered. (c) There are two more silver epoxy contacts on the backside of the cantilever (the end of the tuning fork).*

Figure 3.6: *Probe with broken tuning fork for short test. There are only two silver epoxy contacts on the tuning fork, which are covered with Torr seal. Then the probe was covered with the Kapton mask for sputtering, which turned out to be insulating.*

ton mask. This time, the two gold contacts remained insulating even after metal layers were sputtered. Hence, all the 5 silver epoxy contacts on the probe should be insulated before any metallic layers are sputtered.

3.2.3 Annealing

It is relatively easy to cover the two silver epoxy contacts mounting the tuning fork on the ceramic plate with Torr seal. However, covering the other three epoxies with Torr seal using the same method can be dangerous as this may break the cantilever. Hence it is necessary to find another way to make those three silver epoxy contacts stable under high temperature.

According to the manufacturer, the maximum working temperature of the silver epoxy contacts is 250 °C, which is much lower than the temperature ($>$ 300 °C) during sputtering. Hence we suspect the surface topology shifts during the sputtering process, causing the SiO_x layer to be destroyed. In an attempt to circumvent this, the probe was annealed in a

vacuum chamber at 300 °C for 8 hours in order to over-bake the silver epoxy contacts. By doing so, the silver epoxy contacts can lose organic compounds and thus become less mobile inside.

After annealing, the silver epoxy contacts shrank in size, exhibiting a more "metallic" feature (figure 3.7). This may indicate that the organic compounds in silver epoxy contacts disappeared, and thus the inner structure of the silver epoxy contact may be stable. However, circuits were still shorted only after sputtering of metal layers. This could be caused either by the minor residual organic compounds or the porous structure in the epoxies. But due to lack of safe means to insulate the three epoxies near the cantilever, they can always cause the circuit to be shorted when multilayers are directly sputtered onto the probe.

Given the results above, it is sufficient to conclude that the silver epoxy contacts can cause short due to their porosity. We have tried different approaches to insulate the tuning fork excitation circuit from the deposited metallic layers. However, no method so far was successful at doing so. Hence we need to find other solutions to make electrical contacts.

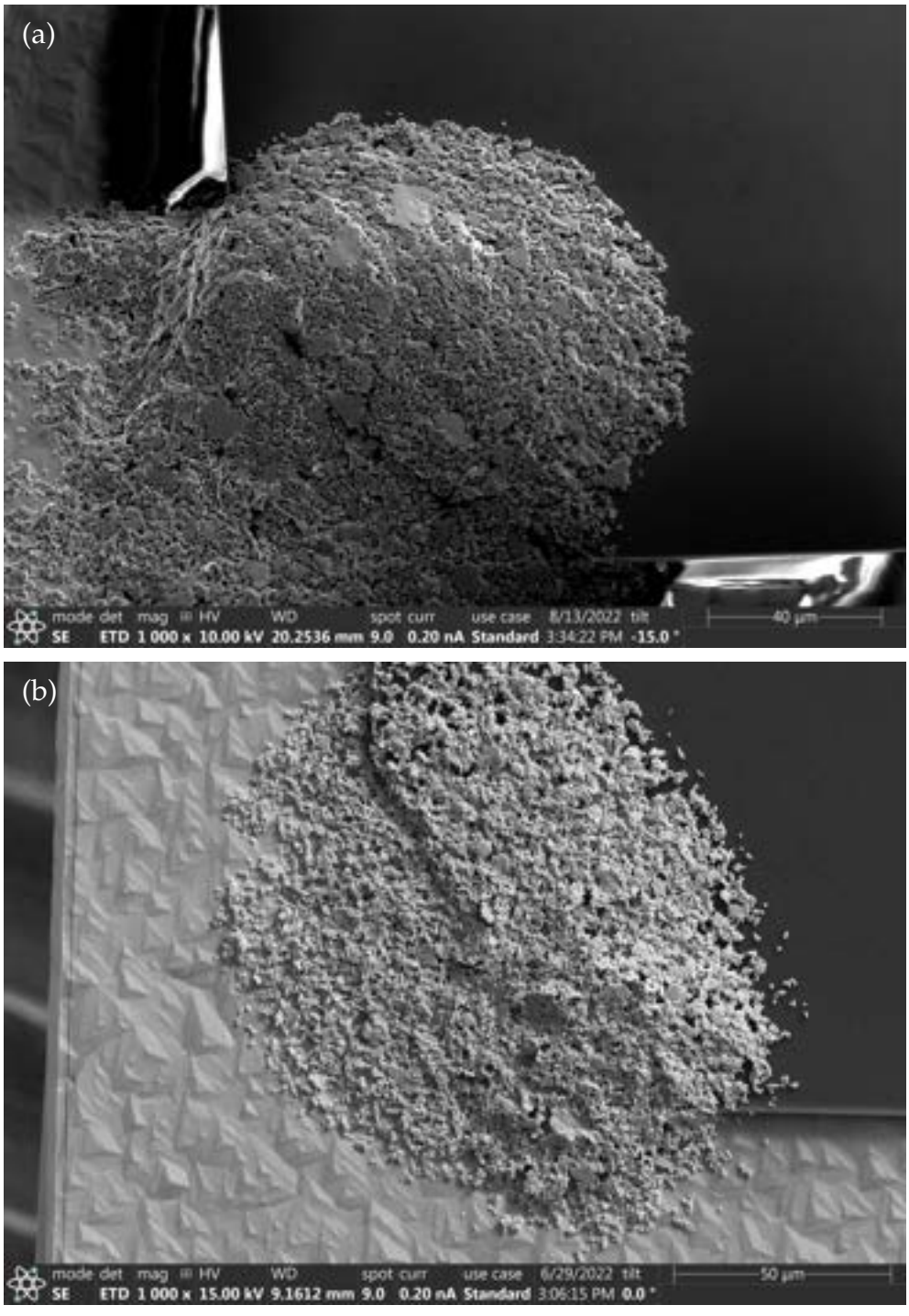

Figure 3.7: *Silver epoxy contact on the front side of the cantilever (a) before and (b) after annealing. The size of the epoxy gets smaller after annealing. The epoxy also looks more "metallic" with more grains of metal after annealing.*

Chapter 4

Method 2: Float transfer

In Chapter 3, we used different approaches to directly sputter multi-layers onto the probe. However, insulation between the tuning fork excitation circuit and SQUID read-out circuit can be compromised due to the defects in SiO_x layer. In this case, high temperature during sputtering enables the change of the inner structure of silver epoxies and their porosity makes insulating layer hard to maintain, which later causes shorts. To avoid these high temperature processes, a float transfer method for depositing metallic layers was explored. This chapter will discuss the results of this effort.

4.1 Introduction to float transfer

As the name implies, float transfer is to transfer layers floating on the surface of a liquid, which in most cases is water, to a substrate. During this process, there are two key factors that ensure the floating layers can be deposited onto the sample. The first is the surface tension force from the liquid. The surface tension can help the floating layers stretch and remain flat. In water, the surface tension force mainly comes from strong hydrogen bonds, which makes water the most suited liquid for float transfer. The second is the van der Waals (vdW) force that adheres the floating layers and the sample. The vdW force is generally much weaker than metallic bonds and other chemical bonds. Hence the surface of the floating layers and the sample should be as flat as possible to have strong enough vdW force.

Figure 4.1 shows the general steps of float transfer. A thin flat layer is used for other layers to grow. This thin flat layer is called the buffer layer. In our experiments the copper layer is a buffer layer that can be etched

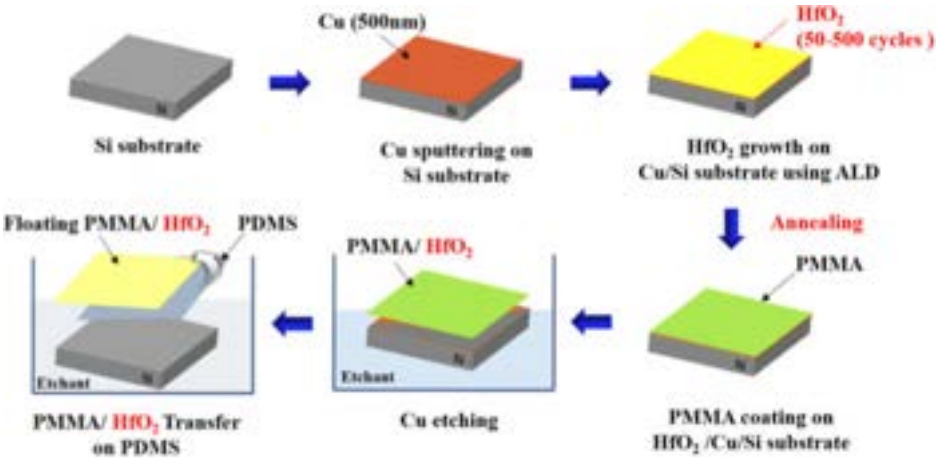

Figure 4.1: *An example of the float transfer procedure. The Cu layer as the buffer layer, which is dissolved by the copper etchant later, is grown on the silicon wafer before other layers. Then the target film (HfO_2 in this case) is grown on top of the copper layer. Adding an extra capping layer of PMMA is to avoid the target film to break apart. After the copper is etched away, the target film will float on water and is ready to be transferred onto the sample. Figure is taken from Y. Kim et al., 2017[19].*

away by some etchant (Ammonium Persulfate (APS) is commonly used in our lab), which enables the target layers to float afterwards. Before the floating layers are transferred onto the sample, they are scooped out and transferred to clean deionized miliQ to remove the copper ions as much as possible. Then the floating layer will be caught up with the sample. After the water on the sample dries up, the layers adhere to the sample.

4.2 Sputtering onto a copper foil

Figure 4.2 shows the general preparation of floating layers. Unlike *Y. Kim et al.* [19], we use a bulk copper foil as the buffer layer since etching thin copper layer from its sides can be a slow process. After all the floating layers are deposited onto the foil, we put the foil in the APS with a concentration of 0.5 Molar. After the copper is etched away, the multi-layers are ready for transfer onto the probe.

Based on this idea, we sputtered multi-layers onto a piece of copper foil (25 μm thick, side length is $\sim$ 4 cm). The sheet of copper with multi-layer on top (Layers-on-Copper, LoC) is too large for spin coating, hence we can only cut off a small piece with side length around 8 mm, which

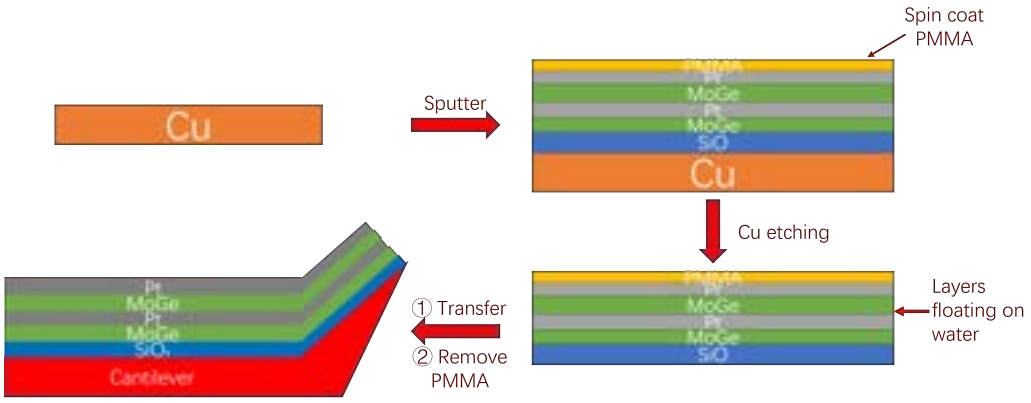

Figure 4.2: *Schematic workflow of the float transfer. The buffer layer is Cu cut from a clean copper foil. Then the copper foil is sputtered with multi-layers. There is a capping layer of PMMA on top to protect the target layers. After the copper is etched away, we can then transfer the floating layers onto the probe.*

is sufficiently large to cover the tuning fork and cantilever of the probe. Since multi-layers are not transparent, it is hard to tell if the copper foil is completely etched away. By cutting off a small piece partly covered with multi-layers and partly with PMMA (indicated as the red dashed box in figure 4.3(b)), we can measure the time needed for the copper to be fully etched away by looking through the transparent PMMA layer. After about 3 hours, there is no brown metal underneath the PMMA layer (shown in figure 4.3(c)), suggesting the buffer layer is fully etched away.

We then tried to transfer the floating layers onto a clean silicon wafer for test. To let water evaporate faster, few droplets of ethanol was added onto the wafer. Then we baked the wafer at 70 °C. However, the water residual boiled and the whole multi-layers did not adhere to the wafer (figure 4.4(a)). Meanwhile, we also noticed that layers peeled off during transfer. As *MoGe* is reactive to APS while *Pt* is not, it is clear that side etching (figure 4.4(c)) happened during the process of copper etching.

From the first float transfer test, we learned that the dry-out process has to be gentle due to the water boiling when heated too quickly. Moreover, it is important to prevent side etching as *MoGe* is the pivotal material in our SQUID.

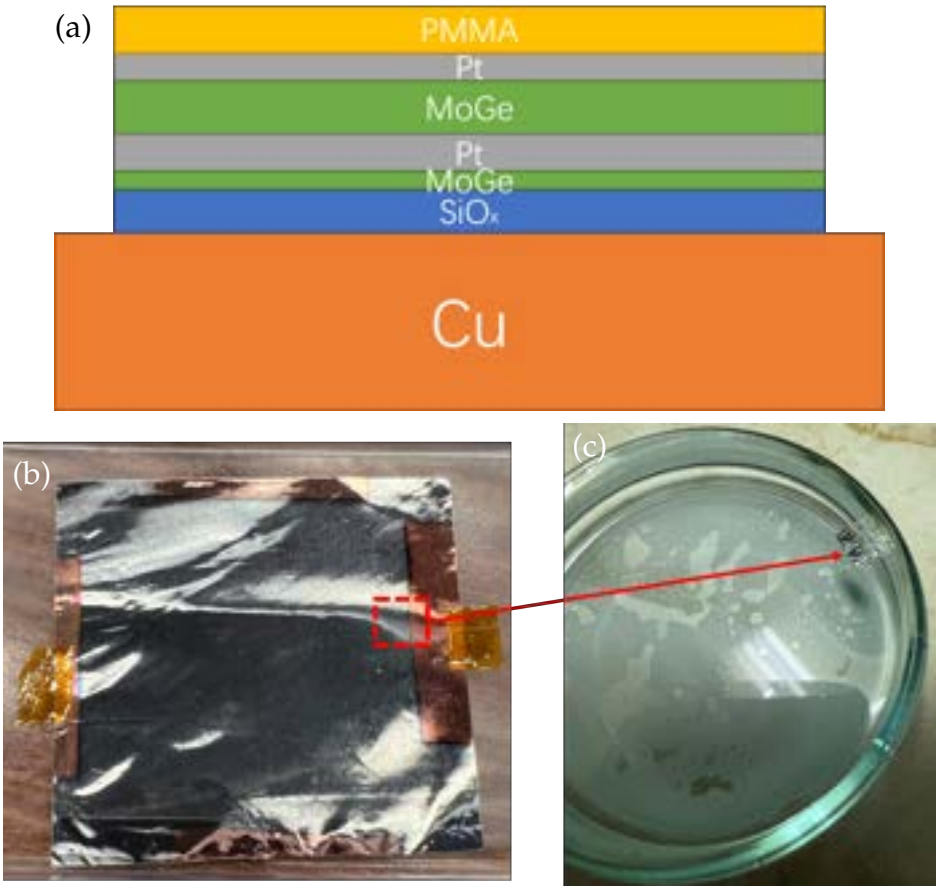

Figure 4.3: *(a) Schematic of the multi-layers structure on copper foil. Here we sputtered* 100 nm *SiO_x for insulation. (b) The appearance of the LoC after multi-layers were deposited, excluding the PMMA layer. The copper foil can bend up and therefore its backside may also be sputtered with layers. So we placed glass slides as weights to flatten the foil in case of sputtering on its backside, which left four unsputtered areas on the four sides of the foil. We then cut off the area marked by the dashed red box and spin coat with PMMA. Since the multi-layered area is not transparent and hence we cannot see if copper is etched away completely. By having a transparent PMMA layer, we can then measure the time for the copper foil to be etched away completely. (c) Multi-layers floating on the APS after copper is fully etched away.*

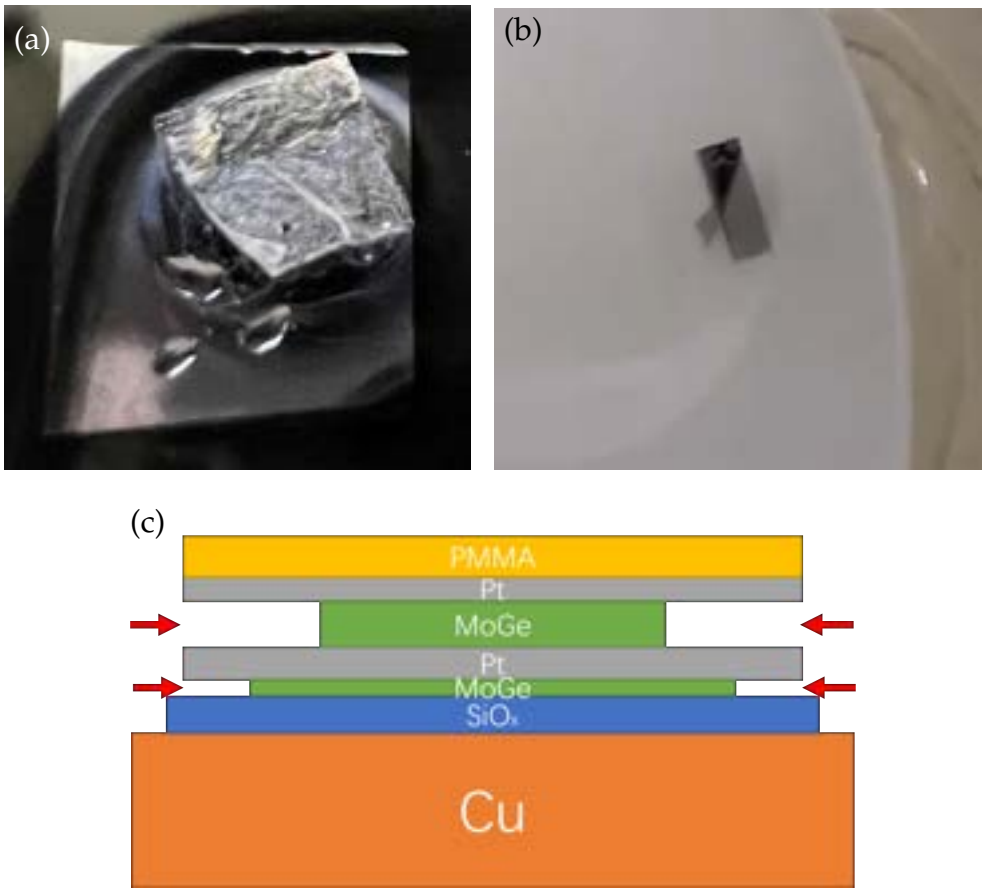

Figure 4.4: *(a) LoC on the silicon wafer. There is no layer adhered to the wafer after adding ethanol and baking out for faster dry-out. (b) Layers peeled off during transfer, which indicates side etching might happened as MoGe is reactive to APS. (c) Schematic of side etching. Red arrows indicate the side etching of MoGe layers.*

4.3 Encapsulating the multi-layers

One way to prevent side etching is to cap the sides of the multi-layers with PMMA, which is not reactive to APS (figure 4.5(a)). To do so, we need to create a margin on the copper foil, which can be done by using silver paint to draw lines onto a large piece of copper foil (figure 4.5(b)). After the multi-layers are sputtered, we can cut a grid off along the red dashed box shown in figure 4.5(c). By removing the silver paint in acetone, multi-layers sputtered onto the silver paint will also be removed and margins will be left on the areas once covered with silver paint (figure 4.6(a)). Then the copper foil with margins will be spin-coated with PMMA, which will

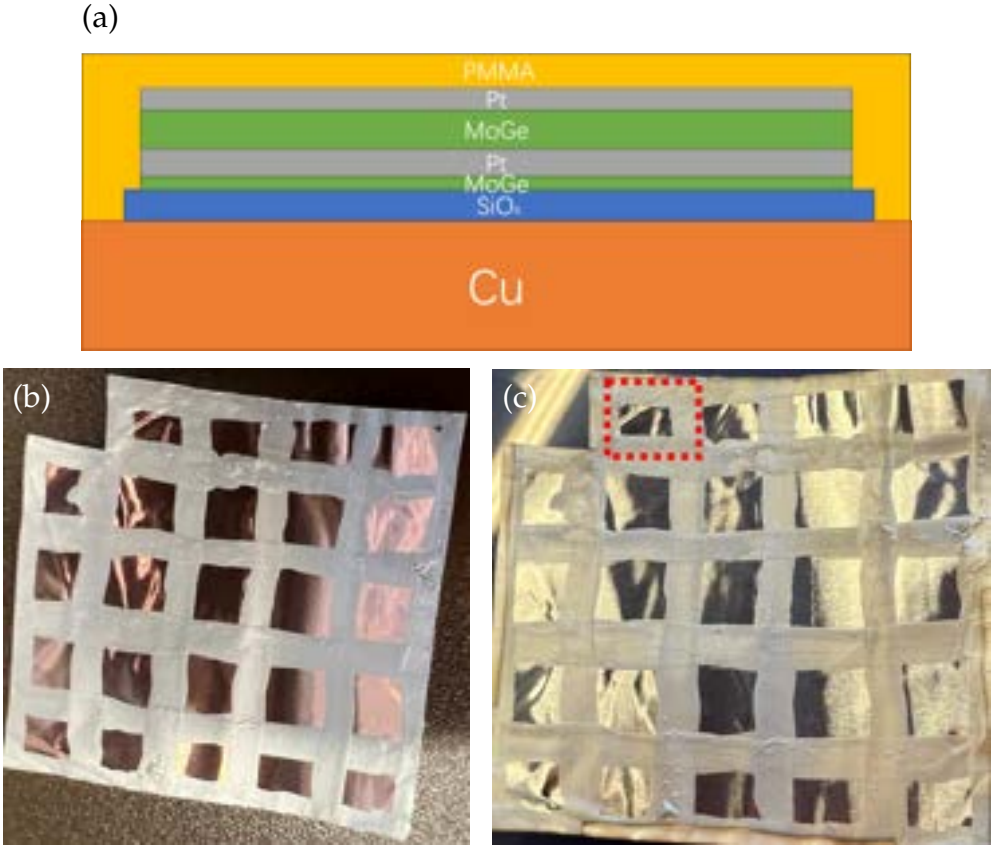

Figure 4.5: *(a) New structure of the floating layers encapsulated by PMMA on copper foil. To obtain such structure, silver paint was used to draw grid lines on the copper foil before sputtering, which is shown in (b). Then after the foil is sputtered with multi-layers (shown in (c)), we can cut along the dashed red box for one floating layer. The silver paint can then be dissolved by acetone to leave margins of the copper foil. After spin-coated with PMMA, the multi-layers will be encapsulated.*

encapsulate the multi-layers.

After the copper foil was etched away (figure 4.6(b)), the floating multi-layers was transferred onto two silicon wafers and air-dried for 30 minutes and annealed at 150 °C for 15 minutes. Then the wafers were rinsed in AR 600-71, which is a remover to remove the PMMA layer, for 1 minute at room temperature and continued with isopropanol (IPA) to remove the remover residuals. Afterwards, the wafers were blow-dried with pressurized nitrogen. During blow-dry, part of the layers came off (figure 4.6(c) and (d)). This is because the floating layers have uneven surfaces, and thus result in wrinkles on the layers. These wrinkles are not attached to the wafer and thus can be blown away easily, and thus we should avoid

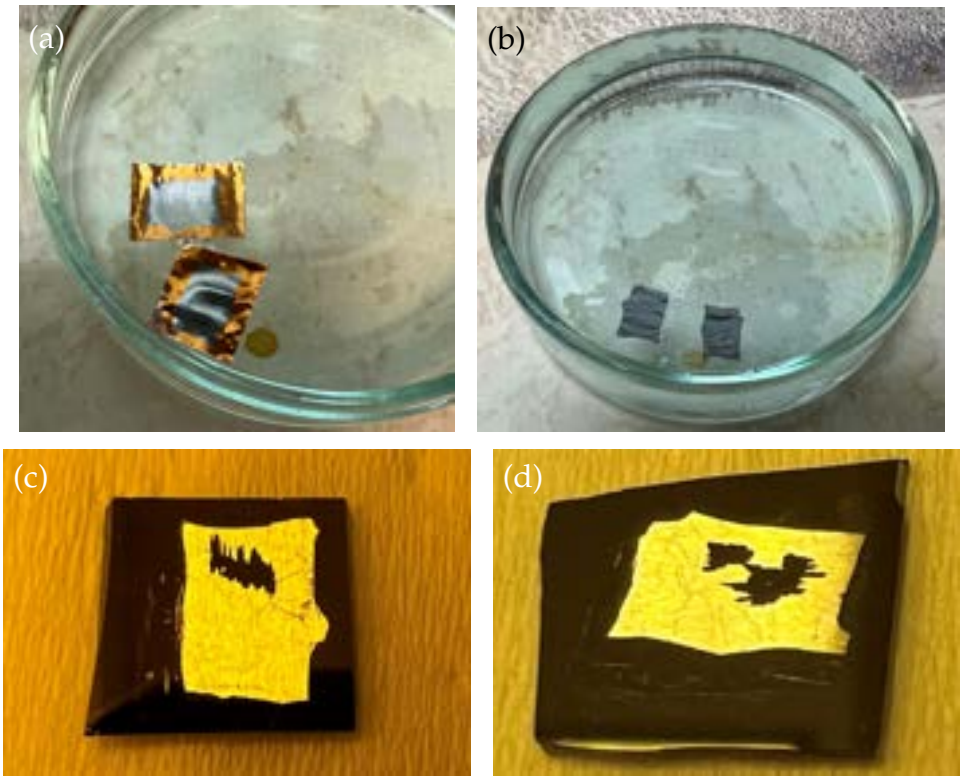

Figure 4.6: *LoC's with margins floating on the APS solution (a) during etching and (b) after etching. There is no layer peeled off. Then the wafers were rinsed in a remover to remover PMMA and IPA to remove the remover residual. (c) and (d) show the multi-layers on silicon wafer after they were blown-dried. Some parts were blown away due to uneven surface (notice the wrinkles), yet most parts remained attached to the wafer.*

blow-dry and let the samples dry out in a more gentle way. Nevertheless, most part of the multi-layers remained well adhered to the silicon wafers, enabling us to transfer layers onto the probes, which has much more complex spatial structures.

4.4 Floating layers on probe

Figure 4.7(a)-(f) show the process of layer transferred onto the probe. During the scooping-out step, we placed the clean probe vertically to let the cantilever catch up the floating layers first. However, it took us several times to eventually have the floating layers placed at the right position. Then the probe was left for air-dry at room temperature for 30 minutes,

followed by 15 minutes of baking at 150 °C. Afterwards, the overhanging multi-layers were torn away using tweezers under the optical microscope (figure 4.7(e)). Then we used a pipette to drop remover droplets onto the probe to wash away the PMMA layer, when the middle part of the multi-layers on the tuning fork was flushed away (figure 4.7(f)).

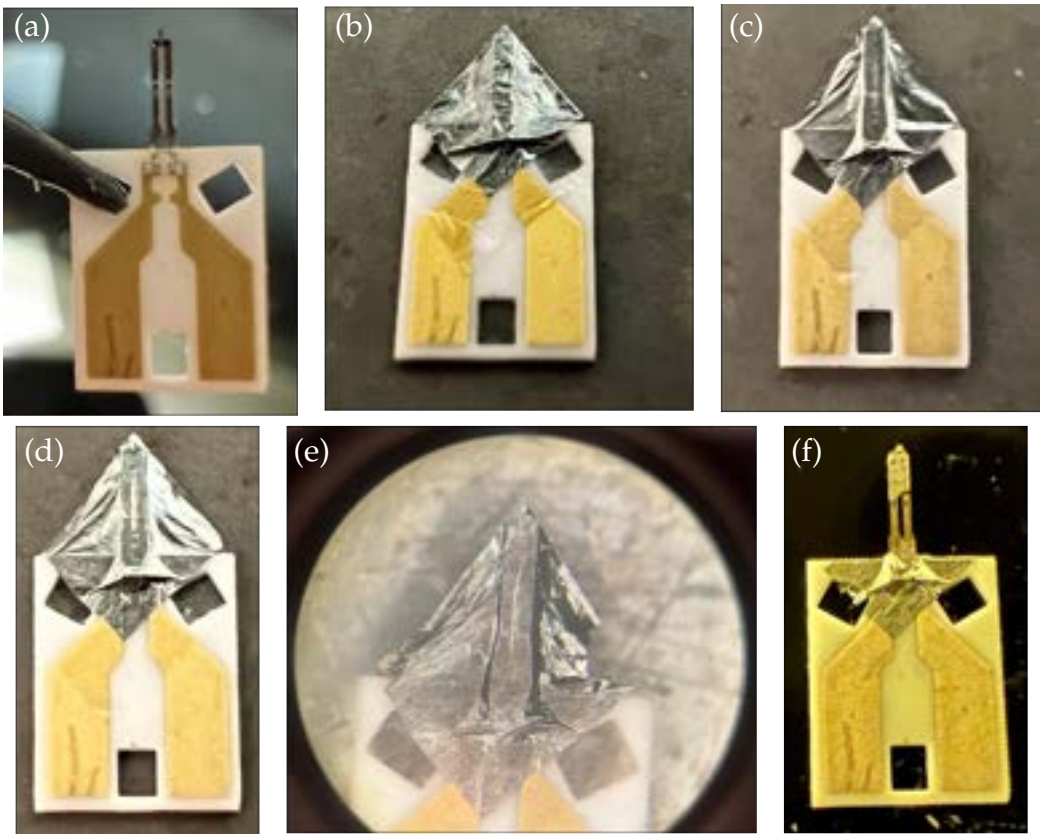

Figure 4.7: *(a) A clean probe before multi-layers were transferred. (b) Floating layers scooped out on the probe. Then the probe was (c) air-dried at room temperature and (d) baked at 150 °C. (e) Tearing off the layers using tweezers. (f) Multi-layers on probe after PMMA removal. Part of the layers went off from the tuning fork, but most part of the layers was still well attached from the end of the tuning fork to the cantilever.*

So far, the multi-layers seem to be well attached to the cantilever, but we need to look at it in the SEM to see if there are multi-layers deposited at the tip. Figure 4.8(a) shows the layer deposition onto the tip. There is a large bulk of multiple stacks of multi-layers near the tip of the cantilever. This could be the result of multiple attempts at scooping out the floating multi-layer when we tried to transfer the floating layers onto the right spot. However, the apex of the tip does not seem to be covered with

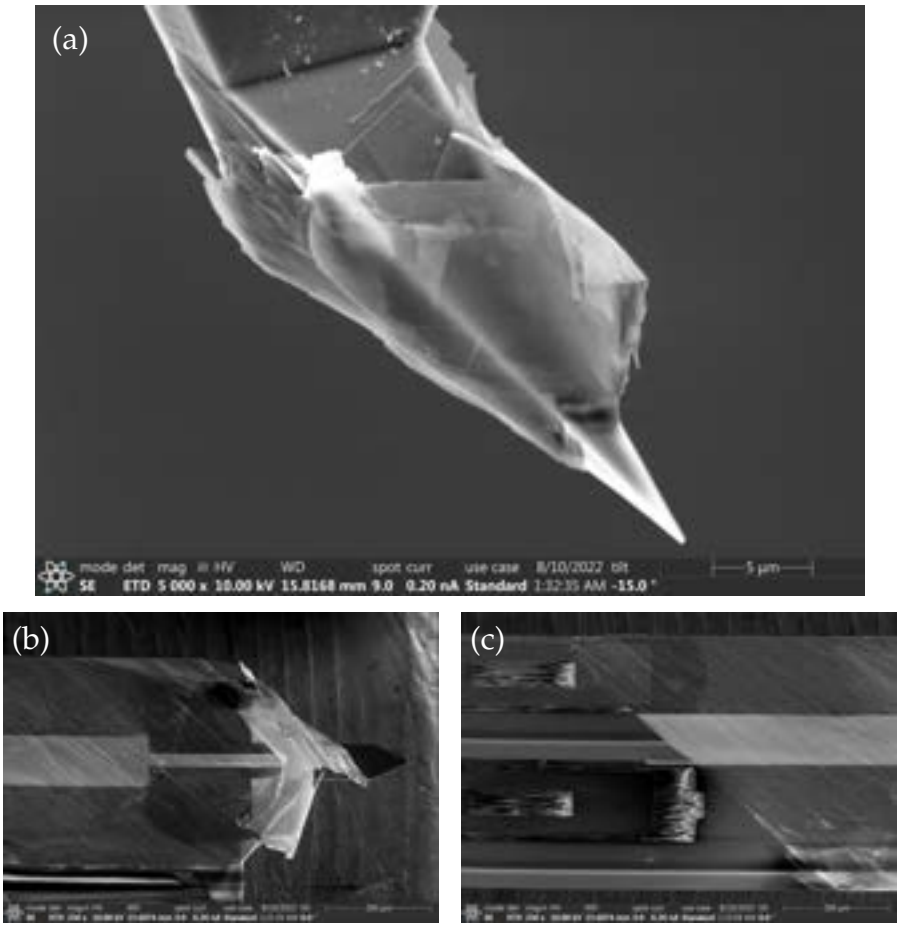

Figure 4.8: *(a) SEM image of the cantilever tip. There are multiple multi-layers attached to the tip, yet there is no layer at the apex of the tip. (b) SEM image of the multi-layers covering the cantilever and (c) multi-layers covering the tuning fork indicate that the layers were still well attached to the probe despite the tip.*

any multi-layers. This could be caused by the tearing of the layers since the apex is small in size and thus the vdW force is too small to hold the layers when external force is applied to tear off the overhanging layers. Nevertheless, as can be seen from figure 4.8(b) and (c), the multi-layers can still attach to the probe firmly aside from the tip apex.

However, the two gold contacts were shorted, suggesting the SiO_x is missing. Since the SiO_x is not as flexible as the metallic layers, it can be broken and compromised during float transfer. This can also allow APS to dissolve the lowest *MoGe* layer. Therefore, we should still sputter the probe with SiO_x directly for better insulation. According to Reference [20], the adhesion can also be improved by placing the sample vertically and

Figure 4.9: *Schematic of conformal adhesion. The orange layer is the target layer and is scooped out slowly by a sample with uneven surface. This will enhance the adhesion between the floating layer and sample. Figure from A. Sharma IITK et al., 2007[20].*

scoop out the floating layer slowly (shown in figure 4.9).

Based on all the known information, we then changed the structure of LoC to what is shown in figure 4.10(a). Then the probe was held vertically to slowly scoop out the floating layers in a conformal way. Then the probe was left for air dry for 16 hours at room temperature[20] without baking. After that, the probe was directly dipped into the remover and IPA gently without tearing the layers (figure 4.10(b)).

Later, this probe was measured for its resistance between the two gold contacts, which turned out to be insulating. Figure 4.10(b) shows that the layers were also well adhered to the probe without adhesive *MoGe* layer. The overview of the layers on the probe in SEM (Figure 4.11(a)) indicates that the adhesion between the multi-layers and probe is still good. Figure 4.11(b) and (c) show that the layers are conformally adhered to the probe despite a large height difference between the tuning fork and the ceramic plate. However, there is still no sign of layers on the tip (figure 4.11(d)-(f)), and only few fragments of the layers are attached to the tip near the apex.

On noticing the striped patterns of the multi-layers in figure 4.8(c) and figure 4.11(c)-(e), it suggests that the copper foil has a stripe-patterned surface due to polishment. This roughness may cause weaker vdW force between the probe and the multi-layers. Furthermore, such pattern can also result in a weaker bonding force perpendicular to the stripes. Hence, the multi-layers can barely adhere to the tip due to the roughness of the copper foil. To obtain a flatter surface for the buffer layer, we then should consider growing copper layer on top of a flat substrate, such as silicon wafers used in Reference [19]. Nevertheless, the float transfer has exhibited its potential of depositing multi-layers onto the probe with considerably good adhesion without creating short between the two gold contacts.

(a)

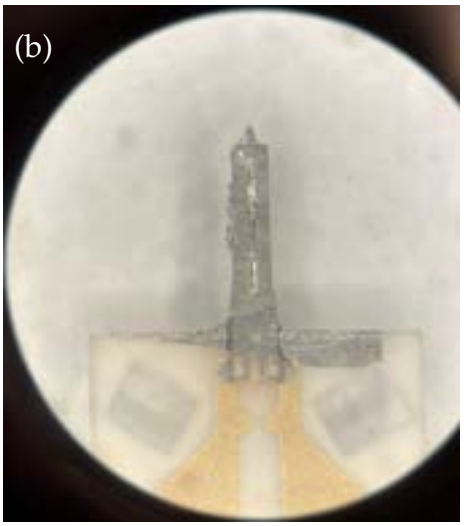

Figure 4.10: *(a) Changed structure of LoC. Both the SiO_x and MoGe layers are removed. (b) Overview of the probe after PMMA removal. The multi-layers seem to be well attached to the probe with minor layer damage.*

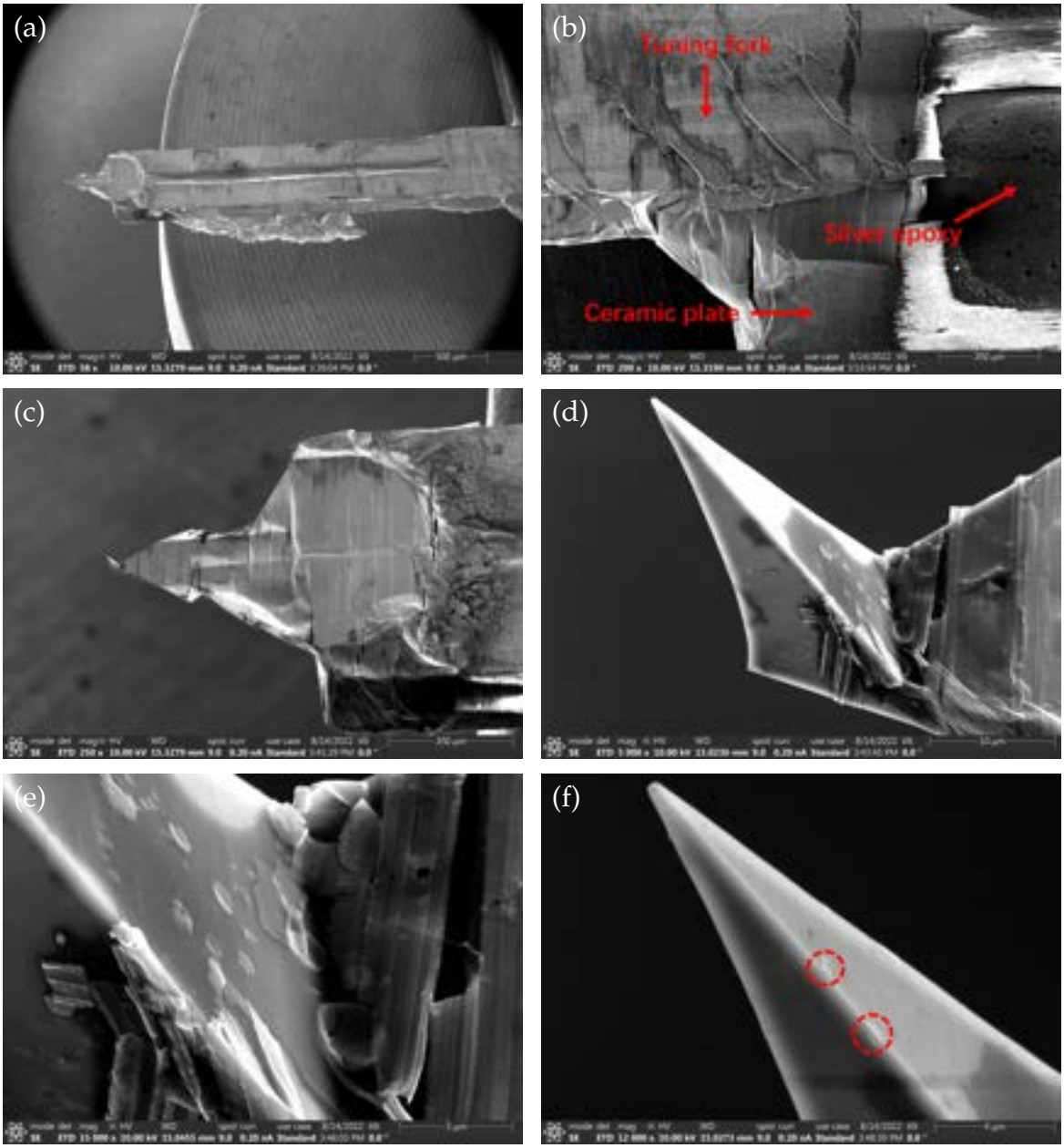

Figure 4.11: *(a) Overview of the multi-layers on the probe. (b) Multi-layers covering the tuning fork and ceramic plate. This indicates good adhesion of the layers even at the presence of a large height difference between the tuning fork and ceramic plate. (c) Overview of the cantilever. (d) Overview of the tip. The tip still seems to be not covered with the multi-layers. (e) Tip foot and (f) tip apex show that there is no layer on the tip despite some fragments of layers at the tip (marked in red dashed circles).*

Chapter 5

Conclusions and Outlooks

In conclusion, we firstly tried to sputter multi-layers directly onto the probe with a hard mask. But this approach requires thorough insulation of the silver epoxy contacts which could not be achieved within the scope of this project. Then to separate the silver epoxy contacts from the multi-layers, we applied PMMA as well as Torr seal and Kapton masks, which did not provide sufficient insulation. A short electrical test involving the separation of the cantilever from the TF indicated that indeed the silver. This indicates that those 5 silver epoxies on the probe is indeed causing shorts. In an attempt to stabilize the integrity of the silver epoxy contacts, the probe was annealed. However, this approach was insufficient as a result of the porous structure of the epoxies.

Then deposition of the multi-layers via float transfer was performed. During this process, there are several factors that play roles in layers-to-sample adhesion. By preparing both sample and multi-layers with flatter surfaces, scooping out the floating layers at a lower rate and dry out the sample naturally, the adhesion can be much improved. Meanwhile, the structure of multi-layers should be changed to avoid side etching. The key findings can be summarized thusly:

- The surface of the copper buffer layer should be as flat as possible, preferably grown on the silicon wafer;
- PMMA can be both capping and capsuling layer to prevent the layers from breaking apart as well as side etching by APS;
- Fewer attempts at scooping out the floating layers prevents less stacking of multi-layers;
- Lower scooping-out rate improves adhesion;

- Air-drying probes after scooping out improves adhesion;
- Multi-layers are too fragile for any external forces.

The transferred layers exhibit good adhesion to the probe. However, this approach is not suitable for layer deposition since there is no layer adhered to the cantilever tip. Nevertheless, adhesion can be improved by growing a flatter buffer layer of copper on the silicon wafer. Alternatively, we can still create conducting contacts all way up to the tip with the two gold contacts insulated using float transfer. This enables easier electrical contacts to the SQUID loop on the tip, which may be developed using other techniques. One possible solution for this is to print electron beam induced deposition (EBID) SQUIDs on the tip and conducting wires to the foot of the tip, which can be then connected to the multi-layers.

Another way to obtain multi-layers on the probe without destroying the insulting SiO_x layer can be using an off-axis sputtering system, where samples are sputtered under much lower temperature with a slower layer growth rate. Or we can also evaporate Nb onto the probe since evaporation is directional and lower temperature is involved. But this might result in lower working temperature of the SQUID because of lower T_c of Nb, which makes cooling down to the working point difficult. Also, instead of using the Akiyama-Probe, there are also some planar AFM probes with two separate arms. These probes could be easier to handle since there is no silver epoxy, yet the spatial resolution might be lower as the tip is less sharper than the Akiyama-Probe.

Chapter 6

Acknowledgement

It is with much pleasure and gratitude to acknowledge my sincere thanks to the help, support and encouragement that motivate my project and further study in physics.

First of all, I would like to thank Kaveh Lahabi, Jan Aarts, and Wolfgang Löffler who have been great supervisors and patient supporters all the time. This project has stimulated my great interest and encouraged me to continue the research on superconductivity. I am especially grateful for Kaveh's full support, without which I would not be brave enough to try my own ideas and build up self-confidence. Their support and guidance have helped me gain much more knowledge than I have ever learnt from textbooks, and I have never enjoyed countless all-nighters trying to find the right path for the experiments ever before this project.

Jimi de Haan has always been a great researcher and friend to me. His keen observation and skilled lab experience have helped me clear lots of obstacles lying in front. Outside working time, Jimi is also a great mental mentor who relieved my anxiety. Working with Jimi has never bored me for a single second.

And I would like to thank my predecessors as well as my good friends, Matthijs Rog and Dennis Uitenbroek. They designed the pivotal theories and experimental process successfully, on which my research is mainly based. Academic talks with Matthijs are always enjoyable. He is great at envisioning about experiments, which saved me from going to dead ends for a lot of times.

I would also like to thank Norman Blümel and Peter Neu for their advice on float transfer experiments. This helped me pick up the skill in a much shorter time.

I am specially thankful to Douwe Scholma and Marcel Hesselberth for

their technical assistance. They are always helpful and kind to help me with lab trainings and technical problems during experiments.

My research in Kaveh and Jan's group has been very enjoyable. Working on SoT has made me enjoy physics research with my greatest interest. With the end of this project showing in sight, my time in Leiden will also come to an end. During my three-year stay in Leiden, I've had the most unforgettable experiences in this city. I love the atmosphere here, where people are like families and academic debates are always refreshing.

There is a Chinese quote from the university where I obtained my Bachelor's degree two years ago,

宇土茫茫，山高水长，为世界之光,

saying that ***The world is never small, and we should never stop seeking for the light of truth of everything***. As we are the light for the future, I sincerely hope my dearest friends and I can be the light that chase after the truth of the universe and feel the awe of the world.

In the end, I would like to thank my family for their love and support.

Bibliography

[1] John R. Kirtley and John P. Wikswo. Scanning squid microscopy. *Annual Review of Materials Science*, 29(1):117–148, 1999.

[2] Y P Pan, S Y Wang, X Y Liu, Y S Lin, L X Ma, Y Feng, Z Wang, L Chen, and Y H Wang. 3d nano-bridge-based SQUID susceptometers for scanning magnetic imaging of quantum materials. *Nanotechnology*, 30(30):305303, may 2019.

[3] Amit Finkler, Yehonathan Segev, Yuri Myasoedov, Michael L. Rappaport, Lior Neeman, Denis Vasyukov, Eli Zeldov, Martin E. Huber, Jens Martin, and Amir Yacoby. Self-aligned nanoscale squid on a tip. *Nano Letters*, 10(3):1046–1049, 2010. PMID: 20131810.

[4] Y. Anahory, H. R. Naren, E. O. Lachman, S. Buhbut Sinai, A. Uri, L. Embon, E. Yaakobi, Y. Myasoedov, M. E. Huber, R. Klajn, and E. Zeldov. Squid-on-tip with single-electron spin sensitivity for high-field and ultra-low temperature nanomagnetic imaging. *Nanoscale*, 12:3174–3182, 2020.

[5] Dorri Halbertal, Jo Cuppens, Moshe Ben Shalom, Lior Embon, Nitzan Shadmi, Yonathan Anahory, H. Naren, Jayanta Sarkar, Aviram Uri, Yuval Ronen, Yury Myasoedov, Leonid Levitov, Ernesto Joselevich, Andre Geim, and Eli Zeldov. Nanoscale thermal imaging of dissipation in quantum systems. *Nature*, 539, 09 2016.

[6] M. Wyss, K. Bagani, D. Jetter, E. Marchiori, A. Vervelaki, B. Gross, J. Ridderbos, S. Gliga, C. Schönenberger, and M. Poggio. Magnetic, thermal, and topographic imaging with a nanometer-scale squid-on-lever scanning probe. *Phys. Rev. Applied*, 17:034002, Mar 2022.

[7] Maria José Martínez-Pérez and Dieter Koelle. Nanosquids: Basics & recent advances. *Physical Sciences Reviews*, 2(8):20175001, 2017.

[8] Carmine Granata and Antonio Vettoliere. Nano superconducting quantum interference device: A powerful tool for nanoscale investigations. *Physics Reports*, 614:1–69, 2016. Nano Superconducting Quantum Interference device: a powerful tool for nanoscale investigations.

[9] P. Reith, X. Renshaw Wang, and H. Hilgenkamp. Analysing magnetism using scanning squid microscopy. *Review of Scientific Instruments*, 88(12):123706, 2017.

[10] Frederick Wells, Alexey Pan, Xian-Jun Wang, Sergey Fedoseev, and Hans Hilgenkamp. Analysis of low-field isotropic vortex glass containing vortex groups in yba2cu3o72x thin films visualized by scanning squid microscopy. *Scientific Reports*, 5:8677, 03 2015.

[11] J. R. Kirtley, M. B. Ketchen, K. G. Stawiasz, J. Z. Sun, W. J. Gallagher, S. H. Blanton, and S. J. Wind. High-resolution scanning squid microscope. *Applied Physics Letters*, 66(9):1138–1140, 1995.

[12] S. Chatraphorn, E. F. Fleet, F. C. Wellstood, L. A. Knauss, and T. M. Eiles. Scanning squid microscopy of integrated circuits. *Applied Physics Letters*, 76(16):2304–2306, 2000.

[13] Y P Pan, J J Zhu, Y Feng, Y S Lin, H B Wang, X Y Liu, H Jin, Z Wang, L Chen, and Y H Wang. Improving spatial resolution of scanning SQUID microscopy with an on-chip design. *Superconductor Science and Technology*, 34(11):115011, sep 2021.

[14] John R. Kirtley, Lisa Paulius, Aaron J. Rosenberg, Johanna C. Palmstrom, Connor M. Holland, Eric M. Spanton, Daniel Schiessl, Colin L. Jermain, Jonathan Gibbons, Y.-K.-K. Fung, Martin E. Huber, Daniel C. Ralph, Mark B. Ketchen, Gerald W. Gibson, and Kathryn A. Moler. Scanning squid susceptometers with sub-micron spatial resolution. *Review of Scientific Instruments*, 87(9):093702, 2016.

[15] Denis Vasyukov, Yonathan Anahory, Lior Embon, Dorri Halbertal, Jo Cuppens, Lior Neeman, Amit Finkler, Yehonathan Segev, Yuri Myasoedov, Michael L. Rappaport, Martin E. Huber, and Eli Zeldov. A scanning superconducting quantum interference device with single electron spin sensitivity. *Nature Nanotechnology*, 8(9):639–644, Sep 2013.

[16] Yonathan Anahory, Jonathan Reiner, Lior Embon, Dorri Halbertal, Anton Yakovenko, Yuri Myasoedov, Michael L. Rappaport, Martin E. Huber, and Eli Zeldov. Three-junction squid-on-tip with tunable in-plane and out-of-plane magnetic field sensitivity. *Nano Letters*, 14(11):6481–6487, 2014. PMID: 25310273.

[17] E. Marchiori, L. Ceccarelli, N. Rossi, G. Romagnoli, J. Herrmann, J.-C. Besse, S. Krinner, A. Wallraff, and M. Poggio. Magnetic imaging of superconducting qubit devices with scanning squid-on-tip. *Applied Physics Letters*, 121(5):052601, 2022.

[18] Akiyama-probe technical guide. https://www.akiyamaprobe.com/AKIYAMA-PROBE_TechnicalGuide_v2.pdf. Accessed: 2022-08-30.

[19] Hyun-Ju Choi and Yongseong Kim. Elastic modulus of hfo2 thin film grown by atomic layer deposition with wrinkle-based measurement. *Bulletin of the Korean Chemical Society*, 38(10):1246–1249, 2017.

[20] Rabibrata Mukherjee, Manoj Gonuguntla, and Ashutosh Sharma IITK. Meso-patterning of thin polymer films by controlled dewetting: From nano-droplet arrays to membranes. *Journal of nanoscience and nanotechnology*, 7:2069–75, 07 2007.